CINTAL - Centro de Investigação Tecnológica do Algarve

Universidade do Algarve

Vector sensor engineering test

EMSO'21

F. Bozzi, F. Zabel, F. Louza, G. Spadoni, R. Duarte,

D. Pozzatti and S. Jesus

Rep 02/22 - SiPLAB
25/February/2022

University of Algarve
Campus de Gambelas
8005-139, Faro
Portugal

tel: +351-289800131
cintal@ualg.pt
cintal.ualg.pt

Work requested by	EMSO-PT - European Multidisciplinary Seafloor Observatory Portugal
Laboratory performing the work	SiPLAB - Signal Processing Laboratory FCT, Campus de Gambelas, Universidade do Algarve, 8005-139 Faro, Portugal www.siplab.fct.ualg.pt
Project	EMSO-PT - European Multidisciplinary Seafloor Observatory Portugal
Title	EMSO'21 vector sensor engineering test
Authors	F. Bozzi, F. Zabel, F. Louza, G. Spadoni, R. Duarte, D. Pozzatti, and S. M. Jesus
Date	February 25, 2022
Reference	02/22 - SiPLAB
Number of pages	50
Abstract	The EMSO'21 experiment was performed from 9h00 to 15h00 on November 24th, 2021. The pressure-gradient vector sensor GeoSpectrum M35 was tested, and its data was collected by an autonomous recorder developed by Marsensing Lda. The field experiment involved a bottom tripod with the M35 and the designed recorder. A Lubell 916C sound source was deployed from the PUMA catamaran, either at fixed locations or towed along isobathymetric or ascending-bathymetric routes. A CTD was used to gather the sound speed in the water column, where local water depths varied from 13 to 30 m. An overview of the experiment and initial data analysis are shown.
Clearance level	UNCLASSIFIED
Distribution list	SiPLAB, CINTAL, IPMA
Attached	None
Total number of recipients	3 (three)

Approved for publication

A.B. Ruano

President Administration Board

Foreword and Acknowledgment

This work was performed under the European Multidisciplinary Seafloor Observatory Portugal (EMSO-PT) project, where acoustic vector sensors were purchased from GeoSpectrum Technologies Inc. The acoustic data were collected using an autonomous recorder developed by Marsensing Lda., which has demonstrated success for recording the vector sensor outputs. The authors would like to thank the SIPLAB participants F. Zabel (data acquisition and deployment support), F. Louza (experiment notes and drone photos), G. Spadoni (experiment notes), R. Duarte (experiment notes and CTD deployment and documentation), and D. Pozzatti (data acquisition and deployment support), and the support of the on board PUMA crew during the experiment. F. Bozzi thanks the support of the Brazilian Navy Postgraduate Study Abroad Program, Grant No. Port. 227/MB/2019.

intentionally blank

Contents

List of Figures

intentionally blank

Abstract

An underwater acoustic communications experiment took place out of Vilamoura harbor to quantify vector hydrophone performance when used as a receiver for UWAC. The experiment was performed from 9h00 to 15h00 on November 24th. The pressure-gradient vector sensor GeoSpectrum M35 was tested, and its data was collected by an autonomous recorder developed by Marsensing Lda. The field experiment involved a bottom tripod with the M35 vector sensor and the designed recorder. A Lubell 916C sound source was deployed from the PUMA catamaran, either at fixed locations or towed along isobathymetric or ascending-bathymetric sailing routes. A CTD was used to gather the sound speed in the water column, where local water depths varied from 13 to 30 m. An overview of the experiment and initial data analysis are shown, where spectrograms, Direction of Arrival estimation, and communication performance enlighten the vector sensor characteristics.

intentionally blank

Chapter 1

Introduction

Underwater acoustic communication (UWAC) systems have recently gained even more importance due to the increasing use of autonomous underwater vehicles (AUVs) [1]. Such vehicles need to establish a communication link to update their inertial navigation system or to send and receive any other on-the-fly information [2]. UWAC issues are well-known, such as the limited bandwidth, intersymbol interference (ISI), and severe delay-Doppler spread [3]. Solutions to enhance communication performance are also known, where robustness, data-rate, and signal processing complexity are conflicting issues. The goal is to reach the fastest possible data-rate with the highest confidence using a low-complexity processor (i.e., lowest power required). However, time and space underwater channel variability makes designing a one-fits-all communication system difficult. Thus, each application (static point-to-point, moving platforms, multiple transmitters-receivers) requires a specific design taking advantage of the available framework. While warfare or research ships can deploy large and powerful communication systems, AUVs are size and power-restricted. Thus, solutions such as array of sensors over the water column, where beamforming or diversity techniques improve communication performance, may not be feasible for AUVs [4]. In general, light AUVs carry only an acoustic modem composed of one acoustic transducer, where a single pressure sensor is used as a receiver [1]. In this sense, a single acoustic vector sensor may provide a considerable gain compared to a single pressure sensor since such device provides directional information of the sound wave [5].

An acoustic vector sensor (VS) is a compact device that measures pressure and two or three orthogonal directional components [5]. Vector sensors have been widely used for sonar applications, where they mitigate left-right ambiguity problems of line arrays and provide a directional gain even in low-frequency signals (under 300 Hz) [6]. The use of VS for UWAC has reduced literature, especially using experimental data, which motivates the execution of tests involving VS receiving communication signals.

From a theoretical perspective, this field experiment aims to verify the benefits of the VS directional channels for communications, where several source-receiver ranges and directions are tested. For instance, we have tested an isobathymetric sailing route where transmissions are performed in opposite directions. This test may help to understand how each directional channel impacts communication performance. Moreover, transmissions were performed at a radius of 2 km from several directions. This test may help to understand how to efficiently combine the VS channels. Furthermore, continuous transmissions with a moving source were performed where the Doppler effect was noticed. This last test aims to verify and quantify the effect of Doppler Doppler in directional channels.

Chapter 2

Vector sensors

This chapter presents the background on vector sensors necessary for data analysis. Pressure-gradient vector sensors are addressed since the used GeoSprectrum M35 vector sensor is designed with this technology.

2.1 Pressure-gradient vector sensors

The literature presents several definitions for vector sensors, thus making it particularly difficult to understand the physics behind them. Here, we adopted the terminology used by Gabrielson, which noticed the same confusing and inconsistent variety of VS nomenclatures [7]. An acoustic VS refers to a generic device that measures vector properties of the acoustic field, where the VS directional outputs are amplitudes relative to directions. This is probably why authors in underwater acoustics refer to VS as directional hydrophones or vector hydrophones. Notice that a hydrophone is commonly referred to as an omnidirectional pressure sensor, i.e., it provides a scalar measure. The intrinsic directionality of VS can be obtained by pressure-gradient or particle velocity (or its derivatives). In theory, particle velocity can be estimated by pressure gradient as shown by Euler's equation:

$$\nabla \mathbf{p} = -\rho_0 \frac{\partial \mathbf{v}}{\partial t} = -j\omega\rho_0 \mathbf{v}. \tag{2.1}$$

where ∇ is the gradient operator, p is the pressure, ρ_0 is the medium static density, $\mathbf{v}$ is the particle velocity vector, and t is the time. Note that the left-hand side pressure gradient can be obtained using finite-difference or simply subtracting the outputs between two closely-spaced pressure sensors. This is the basic principle of pressure-gradient vector sensors. However, the center and right-hand sides (acceleration and velocity, respectively) represent an inertial measure, where the use of accelerometers is widely employed. Perhaps, these two types of approaches (using pressure-gradient or inertial sensors) are the source of several VS nomenclatures. For instance, refer to a velocity sensor (or particle velocity) when using a pressure-gradient sensor.

The pressure-gradient sensor used in this work has the directional information (for each axis) obtained using a pair of hydrophones, as shown in Fig. 2.1.

Consider two small, closed-spaced, identical hydrophones (say a spacing s, where $s/\lambda \ll$

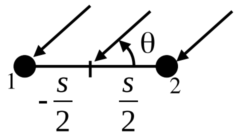

Figure 2.1: Pressure-gradient VS. The hydrophones' outputs are subtracted, forming a dipole.

1) receiving an acoustic wave from θ direction. The subtracted output is given as:

$$\begin{aligned}\Delta p\ (\omega,\theta) &= p_1 - p_2,\\ &= p_0 e^{j\mathrm{k}\frac{s}{2}\cos(\theta)} - p_0 e^{-j\mathrm{k}\frac{s}{2}\cos(\theta)},\\ &= j2p_0 \sin\left(\frac{\mathrm{k}s\cos(\theta)}{2}\right) \to \frac{s}{\lambda} \ll 1,\ \left(\mathrm{k} = \frac{\omega}{c} = \frac{2\pi}{\lambda}\right),\\ &\approx jp_0\mathrm{k}s\cos(\theta).\end{aligned} \tag{2.2}$$

where p_0 is the pressure reference and k is the wavenumber. Thus, the cosine in (2.2) shows the intrinsic directional essence of a pressure-gradient sensor. This sensor is also called dipole vector sensor, 2-D acoustic pressure sensor, when using two orthogonal pairs of hydrophones, or pressure difference directional hydrophone [8, 9, 10]. One can notice that the output is proportional to ks, showing the frequency and spacing dependence, which is drawback regarding the necessary dynamic range. This is the reason why pressure-gradient sensors are considered "aperture" sensors.

The VS output given by (2.2) may not be useful for sound wave direction estimation since a dipole ambiguity is verified. Thus, one hydrophone is used as a reference, usually at the geometric center, resulting in a $(1 + \gamma\cos\theta)$ term, which mitigates the dipole ambiguity according to a design factor γ that may result in a cardiod-like pattern.

Some misunderstanding about the directional pressure measure given by (2.2) comes from its relation to particle velocity, shown in (2.1). Considering a first order differential approximation $\left(\frac{\partial p}{\partial s} \approx \frac{\Delta p}{s}\right)$, the particle velocity from (2.1) becomes:

$$\mathbf{v} = -(j\omega\rho_0)^{-1}\frac{\Delta\mathbf{p}}{s}. \tag{2.3}$$

For plane-waves, particle velocity can be converted to pressure-equivalent particle velocity using $p_v = -\rho_0 c$ v, where p_v is the so-called pressure-equivalent particle velocity and $\rho_0 c$ is the acoustic impedance. Thus, (2.3) becomes for one dimension:

$$\begin{aligned}\frac{p_v}{-\rho_0 c} &= -(j\omega\rho_0)^{-1}\frac{\Delta p}{s},\\ \frac{p_v}{-\rho_0 c} &= -(j\omega\rho_0)^{-1}\frac{jp_0\mathrm{k}s\cos(\theta)}{s},\\ p_v &= \frac{\rho_0 c}{j\omega\rho_0}\frac{jp_0\mathrm{k}s\cos(\theta)}{s},\\ p_v &= p_0\cos(\theta),\end{aligned} \tag{2.4}$$

showing the particle velocity, or its pressure-equivalent, is intrinsically directional. Moreover, (2.4) shows that there is no frequency dependency, differently of (2.2). Thus, in theory, pressure-gradient sensors can lead to particle velocity information. However, the directional measures provided by pressure-gradient sensors are not particle velocity measures, even if we can infer about particle velocity.

Some advantages of this type of VS can be summarized:

- They can be used as a scalar pressure array, which sum of outputs still results in an omnidirectional response, or as a vector sensor by subtracting the outputs;
- Hydrophones can be produced in a very small size, which results in a compact sensor;
- Ideally, hydrophones are insensitive to acceleration (in practice this may not be verified, but comparing to accelerometers they are less sensitive [7]). Thus, they are less affected by mechanical vibrations or noise flow.

On the other hand, pressure-gradient sensors have the following limitations:

- The sensors must have a close response in both amplitude and phase. Thus, it is necessary an accurate design and calibration;
- Since the response is dependent on the spacing between hydrophones, it acts as an aperture sensor. Reducing the size, consequently the spacing between sensors, leads to a decrease in the response. Thus, there is a trade-off between spacing to achieve the dipole-like directionality and a feasible response. Moreover, as close as the hydrophones are, more chance to occur interference (electronic and mechanic) between them;
- Additionally, due to the output subtraction, the dynamic range may be greatly reduced;
- Must have low self noise as the dynamic range is reduced by subtraction. Thus it is required a self-noise reduction design as well;

Chapter 3

Field Experiment

The EMSO'21 vector sensor engineering test took place off the Algarve coast on November 24 th, from 09h00 to 15h00 (GMT+0). Two communication tests were performed using a single VS as a receiver: transmitting at discrete and motionless source-VS ranges and transmitting continuously with source in constant movement. In both tests, the VS is placed at a fixed position.

3.1 Experiment setup and equipment

(a) (b)

Figure 3.1: Filed experiment area and VS tripod position (lat-lon 37.04235°N, −8.16359°W) (a); and the used ship (b).

Figure 3.1a shows an overview of the experiment area, the ship route (detailed range information is given in Fig. 3.4), and the VS position (red dot). Figure 3.1b shows the medium-size catamaran F-122AC-PUMA used in the experiment. The ship left the Vilamoura harbor at 9h00 and went 6 km in the south-west direction where the VS was deployed (lat-lon 37.04235°N, -8.16359°W). Then, the ship route consisted of approximately 2 km around this station (to be described in detail below).

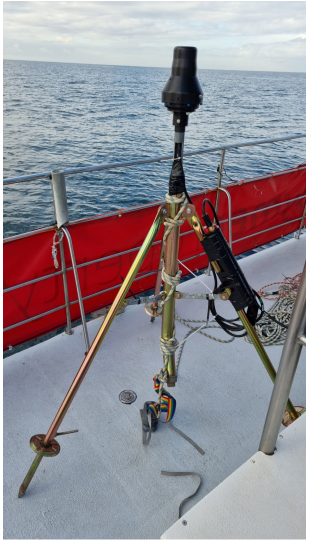

(a)

(b)

Figure 3.2: The M35 VS is placed on top of a tripod, the autonomous recorder is at one of the tripod's legs, and a 10 kg weight is fixed at the tripod center bar to guarantee a vertical deployment (a); the Lubell-916C sound source was used to transmit signals from 4 kHz to 13 kHz (b).

Figure 3.2 shows the used vector sensor tripod assembling (a) and the sound source (b). The GeoSpectrum VS model M35 measures pressure and two orthogonal directional components (x-y components) [8]. The directional measures are estimated by pressure-gradient, and the outputs are compass-resolved, i.e., heading corrected, where the x-component is compensated to North and the y-component to East (see full characteristics in annex I.2.2). The M35 was attached on top of a tripod as shown in Fig. 3.2a. Note that the M35 is heads up since its compass does not works properly upside-down. An autonomous acquisition system designed by Marsensing Lda was attached to one of the tripod's legs and used to record 3-channels of the VS (characteristics in annex I.2.3). A 10 kg weight is fixed at the tripod center bar to guarantee a vertical deployment and avoid that the tripod roll-over due to sea currents. The sound source is a Lubell-916C (Fig. 3.2b), which transmit communication signals from 4 kHz to 13 kHz (characteristics in annex I.2.1).

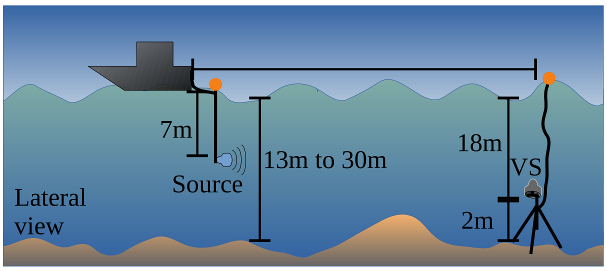

Figure 3.3: Sea trial setup. VS was placed at 2 m from the bottom using a tripod (20 m local depth). The source was tied to a ship at 7 m depth. Several transmissions at discrete ranges were performed. The local depth at these transmissions varies according to the bathymetric map of Fig. 3.4a.

The sea trial lateral view setup can be seen in Fig. 3.3. The VS was placed at 2 m from the bottom using the tripod, where the local water depth is 20 m. The sound source was tied to the stern of the ship either on stations or being towed along a pre-determined track. This sound source was tied at 7 m depth using a rope and an auxiliary buoy.

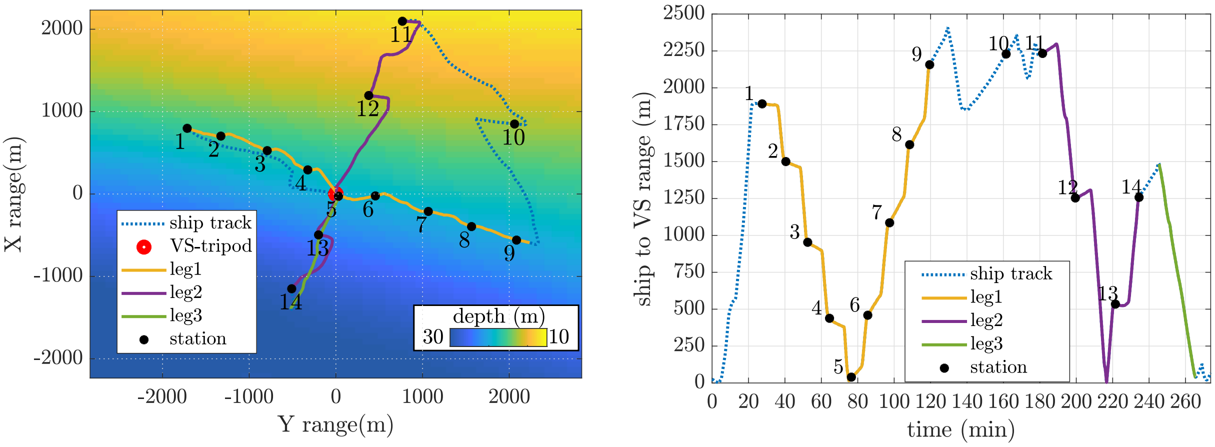

(a) (b)

Figure 3.4: Ship track position and range based on GPS information. X-Y Cartesian plot centralized at VS position is shown in (a) and the source to the VS range along time in (b). In leg1 and leg2 paths, each station indicates a static position where communication signals were transmitted. In Leg3, signals were transmitted continuously with ship in movement.

Figure 3.4a shows the bathymetry of the studied area with the X-Y Cartesian plot, where the VS is at the origin, with latitude 37.04235°N and longitude -8.16359°W. In this VS position the recorder system was turned on, from which the ship goes along stations number 1, 2, up to 14. Figure 3.4b shows the ship to VS range along with time.

In the first test, communication signals were transmitted at discrete source-receiver range (stations). The transmission stations are shown by the black dots and indicated by numbers. Although the idea was to keep static ranges, it is possible to notice movements right after each station in both figures, due to ship drift. Leg1 is a pathway where the water depth is approximately 20 m (isobathymetric), representing a range-independent acoustic scenario. In leg2, the water depth varies from 13 to 30 m, where points 11 to 14 present depths 13, 15, 25, and 30 m, respectively.

In the second test, the source was towed at a speed varying from 2 to 3 knots (1 to 1.5 m/s). Communication signals were continuously transmitted, where the Doppler effect can be investigated. This test interval is represented by leg3, where the ship approaches VS from 1.5 km to 0 m in approximately 20 min. Notice that the ship speed can be considered constant, for this test, according to Fig. 3.4b.

3.2 Transmitted signals

The communication signal used in the first test is shown in Fig. 3.5. From seconds 0 to 243: 4 main blocks (LFMs followed by BPSK) and two JANUS sequences at the end. Before each BPSK block, a probe was used composed of 80 LFM pulses of 20 ms, with 50 ms blank between them. Each BPSK is composed of 50 messages (50 × 2000 random symbols, automatically generated by matlab, see “message_ualg_short.m” in annex I.3)

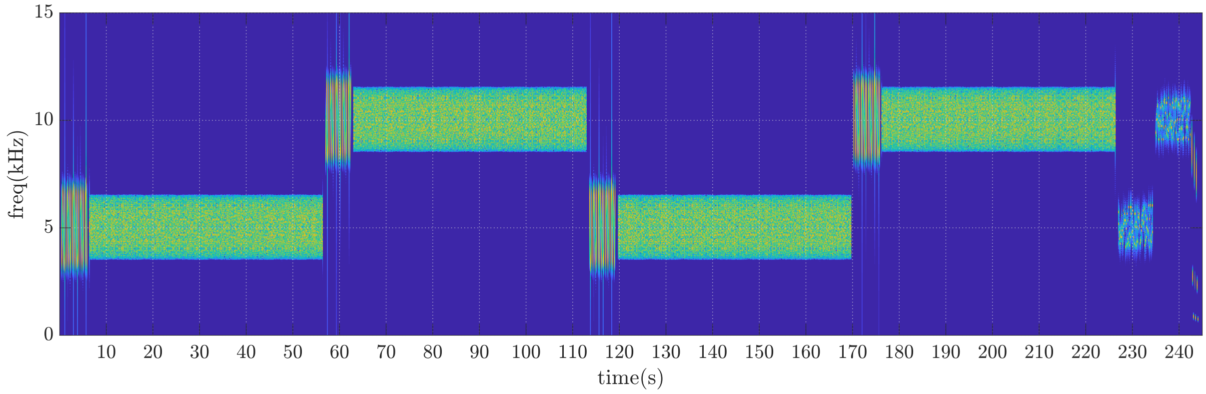

Figure 3.5: Transmitted signal for the first test (leg1 and leg2). Four main blocks (LFMs followed by BPSK) and two sequences using the JANUS protocol at the end.

of 1 s each. For the first and third BPSK blocks, 5 kHz[band:2 kHz] was used, while the second and fourth blocks 10 kHz[band:2 kHz] was used. The first and second blocks use 255 symbol m-sequence preamble in each message, while the third and fourth use 127 symbol m-sequence. The JANUS sequence protocol modulates the phrase "acoustic vector sensors", in the same BPSK bandwidth. In the second test, similar signals were used but the number of messages in the BPSK is reduced from 50 to 10. The m-file of the transmitted signal is available in the project folder (see annex I.3).

3.3 Sound speed profile

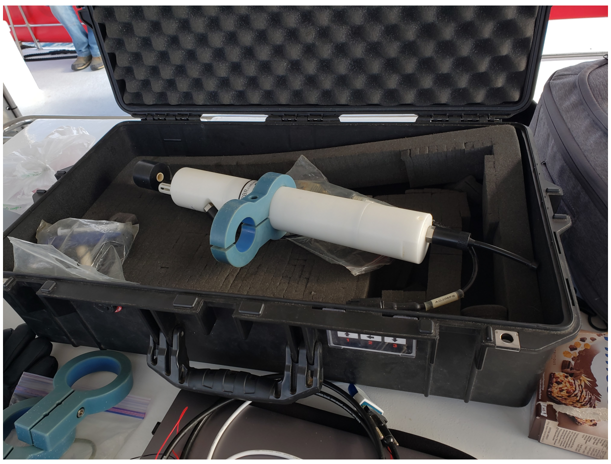

Figure 3.6: CTD model RBRconcerto used during the experiment to obtain the SSP.

The sound speed profile (SSP) was obtained using the CTD model RBRconcerto shown in Fig. 3.6. The main characteristics and the m-file for reading the CTD data are shown in annex I.2.5. Figure 3.7 shows the sound speed along depth for each station. Since the CTD was launched a few minutes before the first transmission for testing, notice that the first two SSP are not named. The CTD was not launched for station 5, so the profile for this station is not available. A vertical red line is displayed referring to 1516 m/s for comparison among profiles. All figures have a grid spacing of 0.5 m/s and a range between

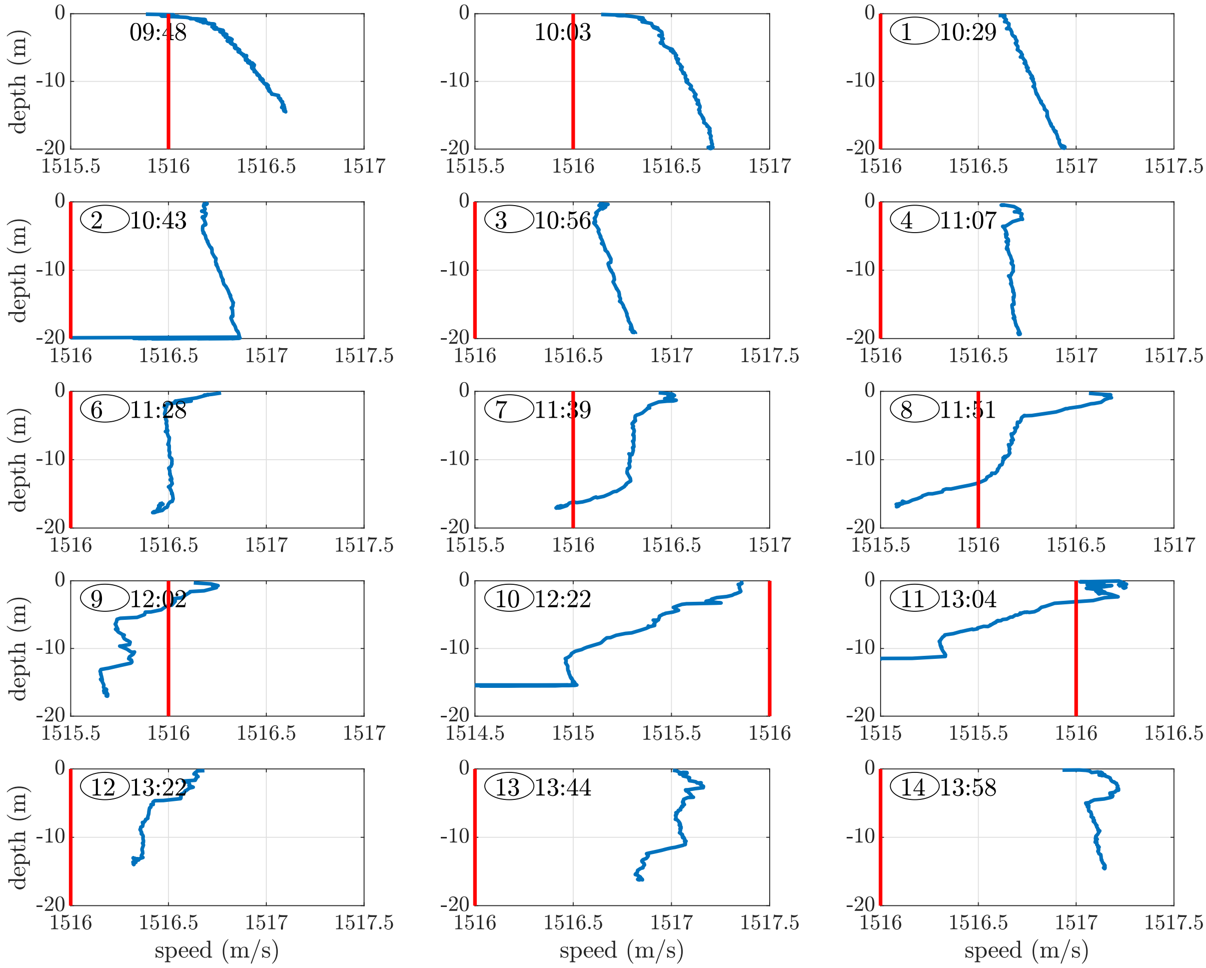

Figure 3.7: Sound speed profile for each station. The two fist profiles were obtained minutes before station 1. The CTD was not launched in station 5. The vertical red lines refer to 1516 m/s (displayed for comparison).

minimum and maximum values of 1.5 m/s. This plot setup seems to benefit comparison among profiles.

The SSP up to station 3 presents an upward characteristic, then an isovelocity is verified for station 4. In station 6, a thin "surface duct" is verified, which becomes a downward profile up to station 12. Then, for station 13 and 14, the mean speed are the highest (around 1517), and the profiles are irregular around this value.

Chapter 4

Preliminary data analysis

4.1 Recorded acoustic signals

In this experiment, an 24-bit resolution autonomous acquisition system records the 3-channels of the VS. This recorder consists of a programmable gain amplifier (PGA), 8-channels synchronous AD converter, in which only three were used, and a microcontroller, used for recording the wave files in a SD card. The PGA was set to the minimum possible gain 1. The sampling frequency is 39062 Hz. The recorder was turned on at 09:58, which is considered the initial time, i.e., minute zero, also considered in the previous GPS analysis.

The recorded signal spectrograms can be seen in Figs. 4.2 and 4.3. In order to provide a clear visualization, we split 4.5 hours recorded in two intervals of 134 minutes, where Fig. 4.2 is the first interval, and Fig. 4.3 is the second. These spectrograms are not calibrated, i.e., they do not take into account the pressure sensitivities. Thus, only a relative reference is given. The spectrograms were calculated using hann windowing with 2048 samples and 256 overlap samples. Considering the same gain for the three recorded channels, the same color normalization was used in the dB scale [-40 0].

Figures 4.2 and 4.3 show pressure channel (a), the North-South component (b), and the East-West component (c). Hereafter, we may refer North-South to the x-component and East-West to y-component for convenience. However, note that x-y axes may not be pointing to North-East since outputs are compass-compensated. The compensation is based on the internal compass aligned to the x-component that estimate the magnetic North. Thus, the output for the North is $p_n = p_x \cos(\theta_n) + p_y \sin(\theta_n)$, and the East is $p_e = p_y \cos(\theta_n) - p_x \sin(\theta_n)$. This operation is equivalent to a rotation matrix. The adopted VS coordinate is shown in Fig. 4.1.

In the first 3 minutes, the vector sensor is outside water causing high-intensity lines in the spectrogram (see Fig. 4.2). The numbers for each station are shown in the spectrogram for guidance. Note that low-frequency noise (under 1 kHz) is more perceptible in the pressure channel. Moreover, comparing the North-South component (in Fig. 4.2b) to East-West (in Fig. 4.2c), higher signal intensity is noticed in the latter. This is an expected result since leg1 pathway are -60° and +100° referred to North, i.e., the ship pathway follows a predominantly West-East direction. DoA estimation analysis will confirm these pathway angles (see Fig. 4.4).

The spectrograms of Fig. 4.2 show the power increase as the source approaches the

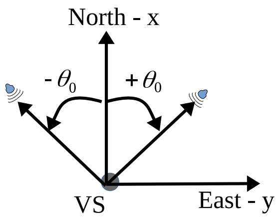

Figure 4.1: Adopted VS coordinates. The directional outputs are north and east compensated. Hereafter, these compensated outputs are referred to x and y components, for convenience.

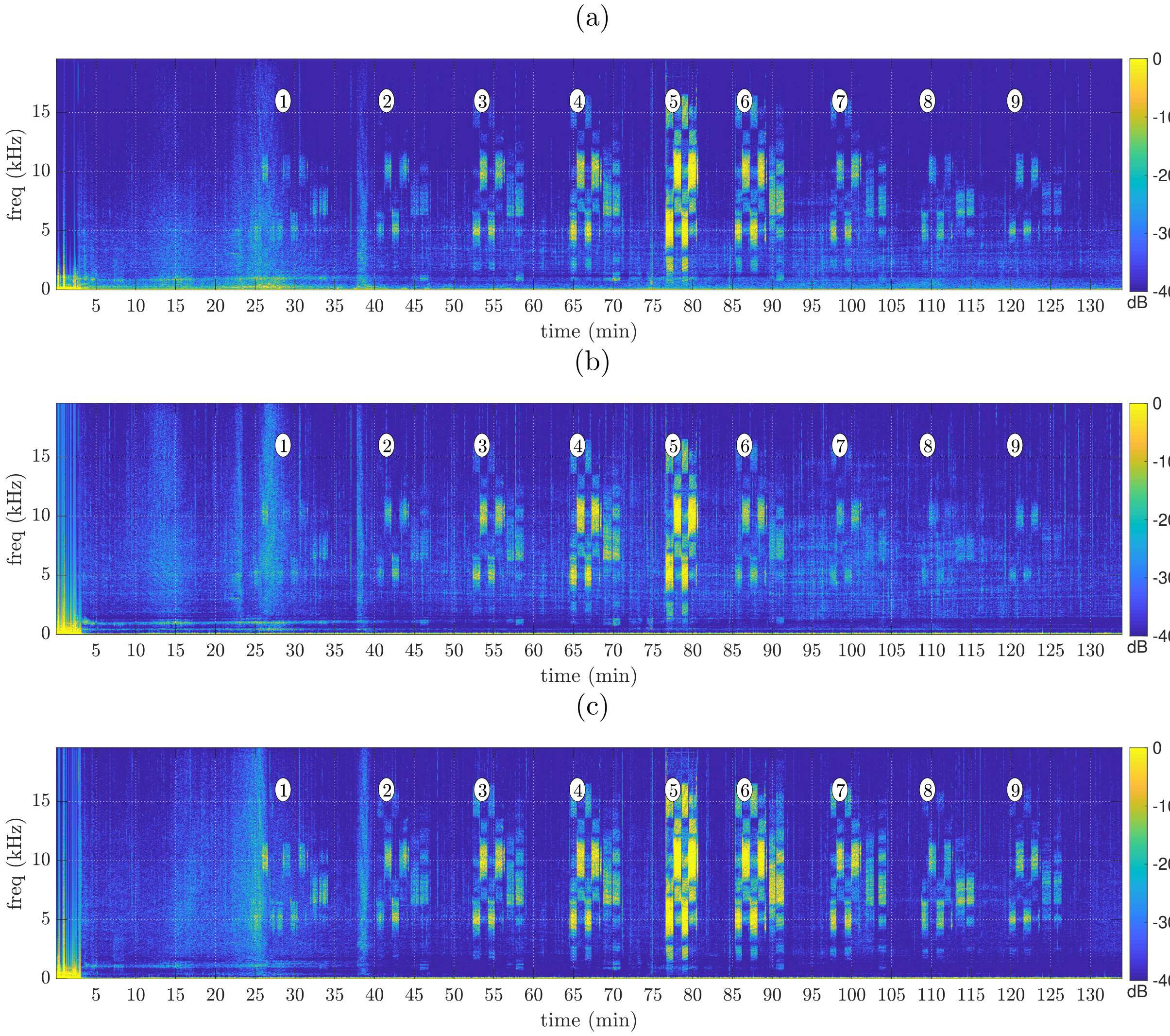

Figure 4.2: Spectrogram (un-calibrated) for pressure (a), North-South (b) and East-West (c) directional components from min 0 to 134 (leg1 - see Fig. 3.4).

VS. According to the GPS range analysis (see Fig. 3.4b), for leg1, the minimum range between source-VS is at min 76, where the 5th transmission was performed. Note that an aliasing-type (around 15 kHz) is present in transmission intervals for close ranges. This is probably due to the source sensitivity, which amplifies signals around 15 kHz (see the source characteristic in annex I.2.1). Notice that the power is largely attenuated for the

North-South component (in Fig. 4.2b), especially for longer ranges. Moreover, this channel presents a higher ambient noise power than pressure/y-component channels, which can be associated to the shore direction.

Figure 4.3 shows the spectrogram from min 134 to 272. One can notice that a transmission was performed at min 140 but it is not displayed at the GPS analysis. In fact, the source power system has presented a failure, this transmission will not be analyzed. Note that from min 120 to min 180, the ship runs counterclockwise from stations 9 to 11, which means it left the West-East direction going to North (see Fig. 3.4). This trajectory change results on a North-South component power increment.

From minute 214 to 219, it is possible to see a noise power increase related to the propeller of the ship passing close to the VS (see Fig. 3.4). Then, transmissions 13 and 14 were performed, which confirmed the North-South component sensitivity. Continuous transmissions of leg3 are shown from minute 250 to 265. At last, it is also shown some spikes in the spectrogram after minute 270, when the VS was removed from the water.

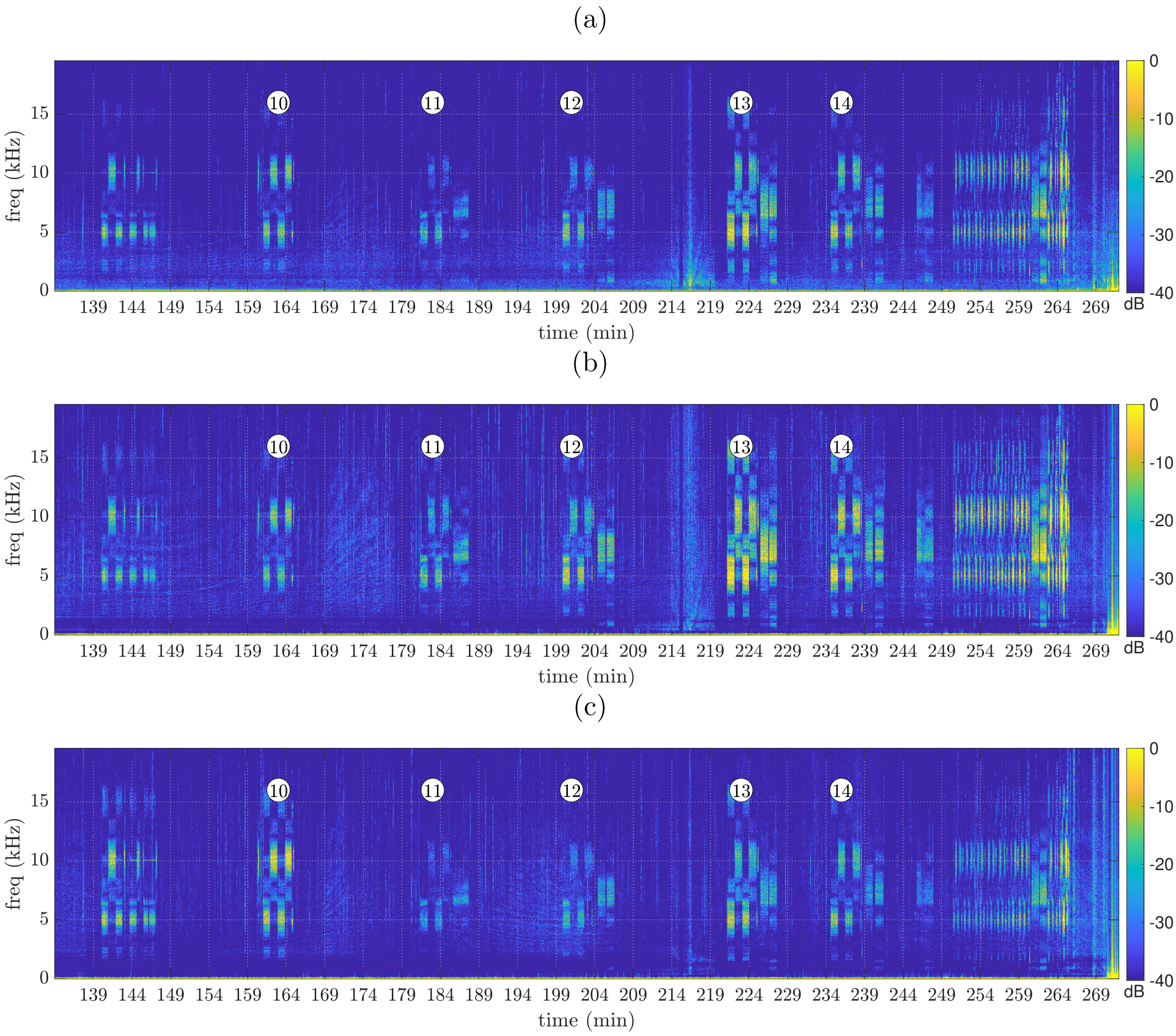

Figure 4.3: Spectrogram (un-calibrated) for pressure (a), North-South (b) and East-West (c) directional components from min 134 to 270 (leg2 and leg3 - see Fig. 3.4).

4.2 Direction of Arrival

Figure 4.4 shows the energy detection using the Bartlett estimator, from which we can obtain an estimate of the Direction of Arrival. The energy integration time is 68 ms, and a threshold of 0.02 for the mean energy of the channels was used to select intervals where transmissions were performed. Thus, the energy displayed in Fig. 4.4 represents ships/transmissions nearby the experiment location over this threshold.

Up to minute 30 fishing vessels were noticed in the region. A small boat passed near the VS at min 37. Our ship has been close to the VS in minutes 77 and 217 (see Fig. 3.4), and it is possible to detect it at these intervals.

The transmission stations are enumerated in Fig. 4.4. An angle comparison can be made between the estimated azimuth angle using GPS info (dashed red line) and the acoustic energy detection. One can notice that spatial aliasing is present but with a small amplitude.

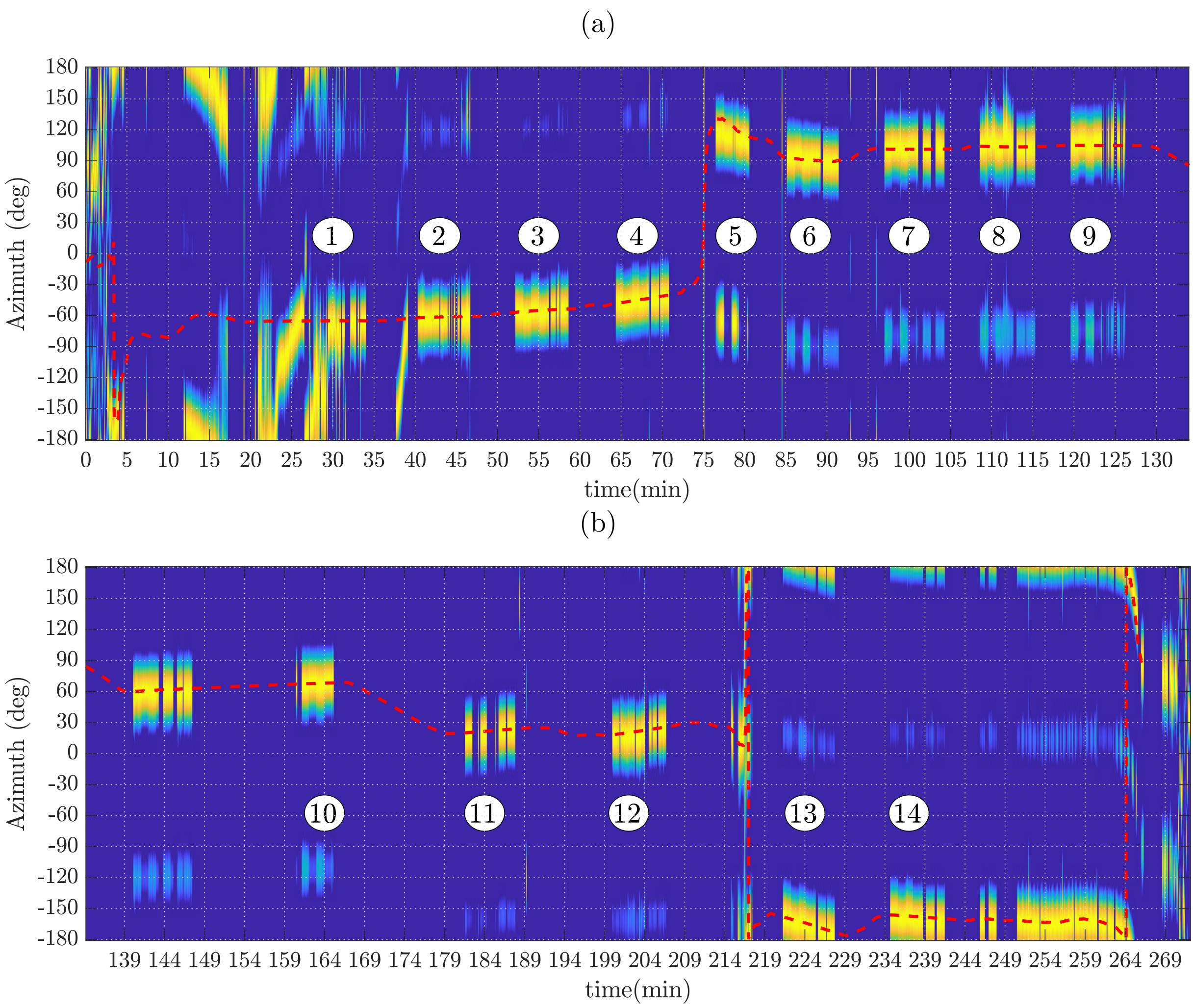

Figure 4.4: DoA estimation from min 0 to 134 (a) and from min 134 to 270 (b). Dashed red line is the estimated azimuth angle based on GPS.

4.3 Communications

This section presents the communication performance. First, we analyze the BPSK modulation for each station of the first test. A further analysis (not shown in this report) aims to quantify the performance for leg3, when the source was moving.

In the following figures, the four results corresponding to each BPSK configuration (see Fig. 3.5). From top to bottom, the performances refer to BPSK configuration: [3 kHz-7 kHz] 255 m-seq, [8 kHz-12 kHz] 255 m-seq, [3 kHz-7 kHz] 127 m-seq, [8 kHz-12 kHz] 127 m-seq. Pressure, x, and y channels are analyzed individually and combined. When combined, three methods are explored: VS equalizer, VS beam steering, and joining both. The VS equalizer (called "vs" in the legend) uses the VS channels as input of a multichannel DFE. The VS beam steering ("bf") weights and combines VS channels, where a single resulted channel (after combination) is the input of a single DFE. The last method ("vsbs") uses both individual VS channels and the beam steered channel as input of a multichannel DFE.

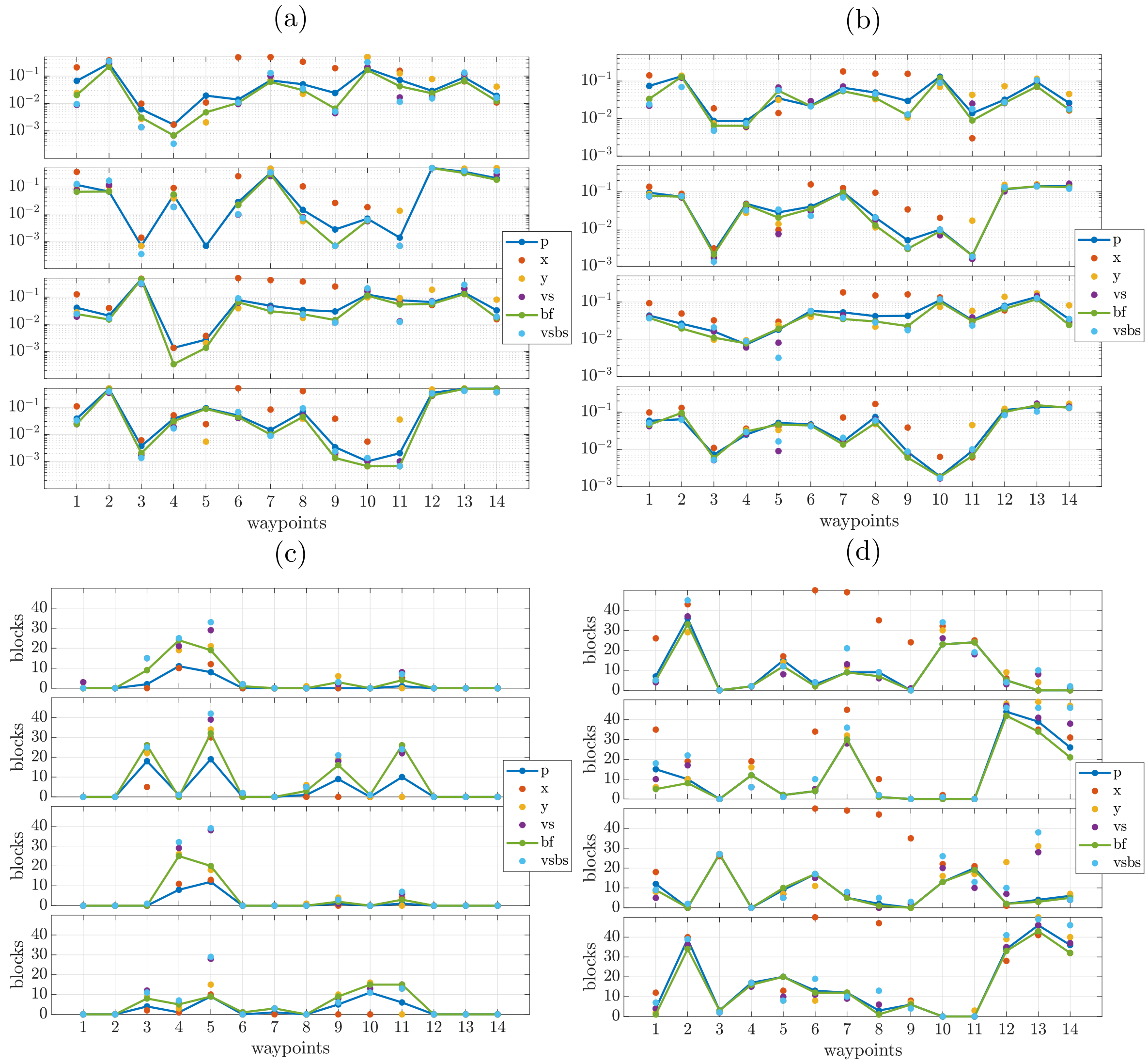

Figure 4.5: BER (a), appropriate BER (b), number of packets that present zero error (c), and number of packets that present error over 20% (d) from station 1 to 14.

Figure 4.5 shows the communication performance for each station of the first test. Keep in mind the West-East trajectory up to station 9. Then, the ship went North, where the source-VS range is approximately 2.2 km for stations 9, 10, and 11. After that, we have the North-South trajectory from stations 11 to 14, where the water depth increases. Since severe fading was observed, the performance presents high variation within the 50 s. Thus, to avoid the impact of outliers we quantify the zero error packets, packets that present error over 20%, and the "appropriate" BER, where errors over 20% are not considered.

Figure 4.5a shows the BER for each station. Individual analysis for each station can be made, however, for now, it is possible to see that VS beam steering (green line) outperforms the single pressure channel. We can also see the impact of directive channels on performance, for instance, the x-component presents a higher error than the other channels when the transmissions are in the West-East trajectory, as expected.

Figure 4.5b shows a slightly better performance using the VS beam steering than the pressure sensor. However, it is important to analyze this figure together with Figs. 4.5c and 4.5d. For instance, looking at stations 9, 10, and 11, we see that the appropriate BER between pressure and VS beam steering is very similar. However, looking at the number of zero and errors over 20%, we can see that VS beam steering presents a better performance. For sure, some results are unexpected, such as the difference in performance between bandwidths. For instance, station 4 presents a lower error using 5 kHz than using 10 kHz. In this sense, the CIR showed in annex II may help the understanding of the performance.

Chapter 5

Conclusion

This report presents an overview and an initial data analysis for the EMSO'21 vector sensor engineering test. The chosen deployment area and sailing route were carefully planned to verify the direction characteristic of VS on communication performance. The developed recorder system from Marsensing Lda works properly, which can be an option for recording signals of this type of VS. The initial analysis provides insight about the VS directional characteristics according to the source direction, verified by spectrograms of each channel. The DoA estimation is in agreement with the GPS information. The preliminary communication performance analysis has shown the expected results, where VS channels were used individually and combined. The relation between performance and direction is clear, and a complete investigation is ongoing to be presented in a future document.

Annex I

Logbook, equipment data sheet, project folder

This annex shows the following topics:

- Logbook table;
- Equipment characteristics: Source, recorder, VS-M35, PASU, CTD;
- Project folder structure;

I.1 Logbook

Time	Event
9h01	Left Vilamoura harbor (heading ± 6 km South-west direction)
9h27	Arrived at the VS deployment position (37°02'31.9"N 8°09'47.3"W)
9h48	CDT launched to test
9h58	Acquisition system (recorder) turned on
10h02	Tripod deployment done (depth 20 m)
10h23	**Station 1** (Noticed several ships/fishing boats on East side of the VS)
10h25	First transmission / CTD launched
10h28	Re-transmission because we though the power was too high. Starting with a lower power (PASU -24Vrms [5 kHz],21Vrms [10 kHz]). Sailing route in East direction
10h41	**Station 2**. Noticed a small boat at South side of our ship going to North direction. CTD launched
10h47	Finished station 2
10h53	**Station 3**. Noticed that the small boat was at West side of our ship going to North direction. CTD launched
10h59	Finished station 3
11h05	**Station 4**. CTD launched. We can see the VS buoy.
11h11	Finished station 4

11h16	**Station 5**. We approach the VS buoy, but not enough to stay over it. The ship was drifting to East. It seems we were at approximately 40 m from the VS buoy. The CTD was not launched.
11h21	Finished station 5
11h26	**Station 6**. It seems that the sea starts to have some undulation (until this station a very flat sea was verified). CTD was launched.
11h32	Finished station 6
11h37	**Station 7**. A cargo ship was seen at South-East side of our ship (faraway). CTD was launched.
11h45	Finished station 7
11h49	**Station 8**. The sea has presented some undulation. CTD was launched.
11h56	Finished station 8
12h00	**Station 9**. CTD was launched.
12h07	Finished station 9. Following on North-West direction.
12h20	**Station 10**. CTD was launched.
12h24	Re-transmission because we noticed that the transmission was interrupted. Something strange happens with the transmission system (PASU). In a first place we though it could be the battery, and changed it, but without success. Finally, the issue seems to be a cable connection problem.
12h40	Transmission station 10. It was noticed that the ship had drift a lot (to East). In this transmission, the ship engine was turned off.
12h46	Finished station 10. Continuing on North-West direction.
13h02	**Station 11**. Our ship turned off the engine during the transmission. CTD was launched. Depth 13 m
13h08	Finished station 11. Following on South Direction
13h20	**Station 12**. CTD was launched. Depth 15 m
13h27	Finished station 12
13h42	**Station 13**. A very light rain started (drizzle). The sea have a stronger undulation. CTD was launched. Depth 25 m
13h48	Finished station 13
13h55	**Station 14**. Depth 30 m
13h59	Finished station 14. Extent the rope length (to the auxiliary source buoy) to approximately 10 m
14h02	**Doppler leg**
14h24	Finished Doppler leg

Table I.1: EMSO'21 sea trail. Additional information can be found in the photos in hand-written format in the project folder

I.2 Equipment characteristics

I.2.1 Acoustic Source

Figure 1.1 shows the Lubell-916C transmission response. We can note that the for higher frequencies (over 3 kHz) the source can present up to 30 dB of attenuation. The transmitted signals use the carrier frequencies of 5 kHz and 10 kHz. In these frequencies (for 1 kHz bandwidth) the source shows a windowing-shape, which the plateau is in the carrier frequency.

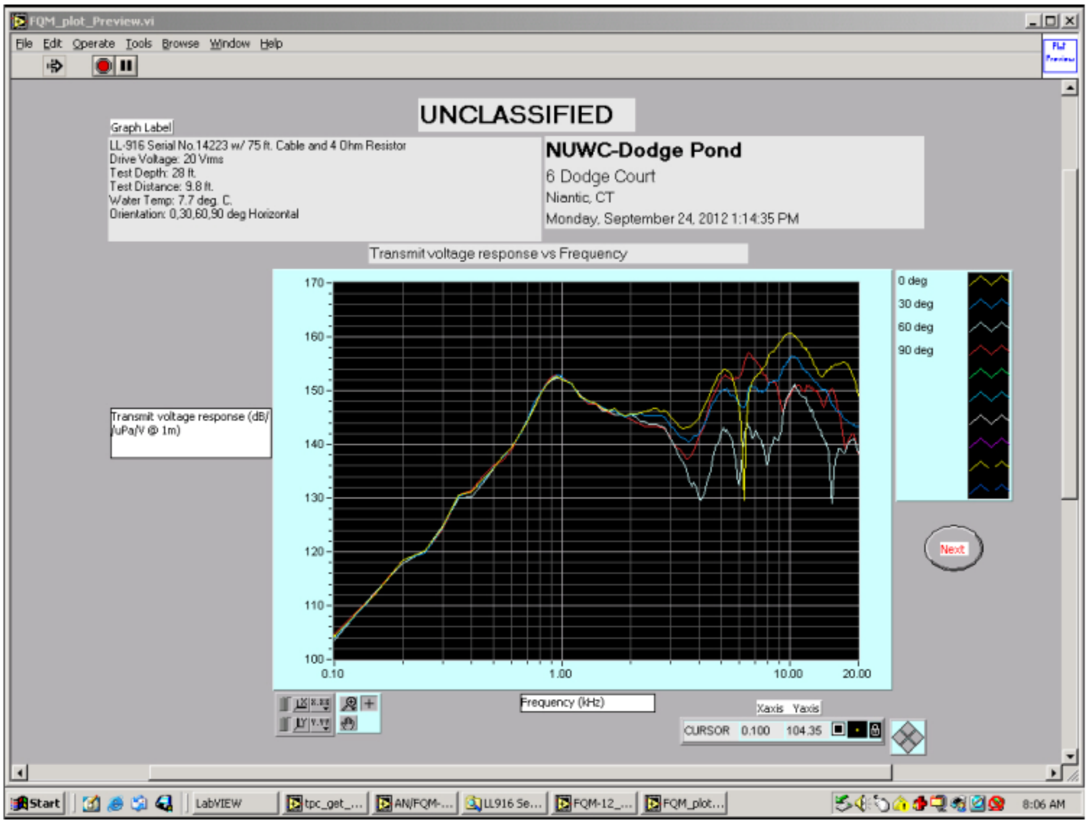

Figure 1.1: Lubell-916C transmission response

I.2.2 VS manual

Essential pages of the VS-M35 user's manual is attached in the following pages for convenience. Notice that the VS-M35 provides differential signals (sec 2.3) preamplified with 36 dB. Note also the heading corrected information shown in sec 3.3.3. Finally, the receiver response for the omnidirectional and directional channels are shown in Figs. 3 and 4 of this manual.

1 Introduction

This document describes the operation and maintenance of the M35-300 directional hydrophone.

Please read this document in its entirety before operating the enclosed system. The M35-350 is a sensitive instrument. The user should have a thorough understanding of its operation and any interfacing equipment prior to use to prevent risk of damaging the sensor. For information not found in this user's manual regarding operation and maintenance specific to the user's application, please contact GeoSpectrum via email (support@geospectrum.ca) or by telephone (902-406-4111).

1.1 Formatting

The following formats are used to highlight key points within the manual. Also, non-standard wording or words that are used to describe specific actions, relationships, or objects are italicized to emphasize this fact.

Tip: A hint to make things easier.

Note: Not a warning, but something that is important to understand.

Warning! Highlights an important feature/item that demands the user's attention.

Stop! Highlights a crucial feature/item that can severely impact performance/usability.

1.2 Suggestions and support

The quality of our products and services is of the highest importance to GeoSpectrum. Should you require application specific recommendations, operator related difficulties or require any additional support, we encourage you to contact us.

Suggestions and support can be reported to GeoSpectrum via email (support@geospectrum.ca) or by telephone (902-406-4111).

2018-468, R1

2 Overview

2.1 M35-300 directional hydrophone

The M35-300 is a directional hydrophone designed to measure 2-D acoustic pressure in a broad range of environments. The M35-300 includes a 2-dimensional orientation sensor, 2 dipole sensors and one omnidirectional acoustic pressure sensor.

Figure 1: M35-300 Directional Hydrophone.

The M35-300 directional hydrophone is shown above in Figure 1. A description of the major components of the hydrophone follows;

2.2 M35-300 Sensor housing

The M35 pre-amplifiers, electronics and orientation sensor are housed in a two-part water-tight anodised aluminum housing. The housing is designed to withstand deployment of the sensor to depths of 1000 m. six blue anodised screws hold the two halves of the housing together and maintain a water-tight seal. An SAE fitting is included on the top cap, this fitting is used in the construction of the M35 and sealed at the factory.

	Warning! DO NOT loosen or remove either the blue anodised screws that hold the two parts of the housing together or the SAE fitting in the top cap. Doing so may compromise the water-tight integrity of the housing.

The top cap of the aluminum housing has four threaded holes that can be used for mounting of the sensor. Drawing 02-035-031, included in Annex B, details the interface arrangement.

Attached to the aluminum electronics housing is the sensor head containing the sensing elements of the Omni and Directional channels. The sensing head is Urethane construction to provide a water-tight, near acoustically transparent barrier.

Note: Care should be taken when handling the sensor not to damage the encapsulation of the sensor head. Sit the sensor on a clean debris-free surface.

2.3 Pre-amplifiers

Both the directional and omnidirectional sensors are wired to pre-amplifiers located inside the M35. The M35-300 pre-amplifiers are differential voltage output signaling with gain and filter settings selectable on order, unless otherwise specified the standard specification is provided in Table 1 with 36 dB of gain and -3 dB filter points of 2 Hz and 20 kHz.

Table 1: M35-300 nominal pre-amplifier characteristics.

AUDIO CHANNEL	PRE-AMP GAIN [dB V] (FLAT GAIN)	LF ROLL-OFF [Hz] (-3 dB POINT)	HF ROLL-OFF [kHz] (-3 dB POINT)	OUTPUT
Omni	36	2	20	Differential voltage
N-S	36	2	20	Differential voltage
E-W	36	2	20	Differential voltage

Each preamplifier has a nominal 2.25 V DC offset on their output and swing 0 V to 4.5 V giving a maximum 9 Vp-p differential output (2.8 Vrms differential / 9 dBVrms). The maximum input level will correspond to the selected gain, however with a nominal 36 dB gain the channels will saturate if the senor input exceeds 125 mVp-p at input of preamplifier. Assuming a peak directional sensor sensitivity of -154 dB re 1 V/µPa @ 10 kHz this equates to a maximum SPL at the sensor of 163 dB re 1 µPa @ 1m.

2.4 M35-300 Electrical connector and extension cable

The electrical connector is a SubConn MCBH8M bulkhead connector. The pin-out for the connector is detailed in drawing 02-035-031, included in Annex B.

An extension cable can be provided with the sensor for deployment, see detail drawing in Figure 6, included in Annex C.

3 Equipment operation

3.1 Omnidirectional and directional sensors

The M35-300 is a hydrophone designed to measure 2D acoustic pressure in a broad range of environments. The sensor includes two orthogonally arranged directional channels and one omni-directional acoustic pressure sensor.

Each of the directional channels are conventional pressure hydrophones arranged to measure the acoustic pressure gradient in one direction. They provide a dipole beam pattern with the Maximum Response Axis (MRA) aligned to the sensor body X and Y axis respectively. Directional outputs are compass-resolved to North and East components within the sensor using an internal orientation sensor.

The direction of signal arrival can be determined using the signal levels from the two directional channels to compute a vector and then compare each directional channel's phase to the omnidirectional channel to determine the correct quadrant in a Cartesian coordinate system.

3.2 Sensitivity and beam-patterns

The nominal receive sensitivity of the M35-300 sensor is shown in Figure 3 Included in Annex A. The response of the Omnidirectional Channel is essentially flat across an operational band of 1000 Hz – 15 kHz. The directional sensor response varies with frequency across the operational band.

An example of the channel directivity is shown in beam-pattern plot Figure 4 included in Annex A.

3.3 Signal description

Warning! Power sensor with a DC supply and a voltage range between **5.0 VDC to 15 VDC**, do not exceed 15 VDC.
Warning! Do not apply DC power to the audio channel pins.

3.3.1 Power - Pin 1

Supply negative (return). Note that this signal is DC isolated from the sensor casing

3.3.2 Power (+) - Pin 2

DC Supply positive. Power sensor with DC supply within stated voltage limits. Maximum draw is 45 mA for approximately 30 seconds after power up, this reduces to approximately 35 mA when the serial interface powers down. This input is reverse voltage protected by an internal self-resetting 0.25 A fuse.

3.3.3 Audio channels – Pins 3 to 8

A description of the three audio channel signals and directional phase relationships is provided below.

All audio signals are centered at half the internal analog supply rail (approximately 2.25 V) and can swing between 0 V and +4.5 V, yielding a differential peak-peak voltage swing of approximately 9 V. The outputs are driven via internal 100 ohm series resistors.

Table 2: Audio Channel Signal Description.

Audio Channel	Pin	Description
Omni (+) Omni (-)	3 4	These two signals are the DC coupled differential analog output of the Omni Sensor signal.
N-S (+) N-S (-)	5 6	These two signals are the DC coupled differential analog output of the heading corrected **North-South** Sensor signal. **Positive phase**, when referenced to the Omni channel signal indicates **North**.
E-W (+) E-W (-)	7 8	These two signals are the DC coupled differential analog output of the heading corrected **East-West** Sensor signal. **Positive phase**, when referenced to the Omni channel signal indicates **East**.

3.4 Deployment

⚠ Warning! The M35 Sensor has is designed to operate to a maximum depth of **1000 m**.

- Do not exceed the maximum operating depth during deployment.
- **M35 sensor is designed to be deployed with the sensor head facing UP and the integrated connector facing DOWN. See Figure 2. Deployment in alternative orientations will result in improper readings from the compass-resolved directional output channels.**

2018-468, R1

Annex A M35-300 Sensitivity and beam-patterns

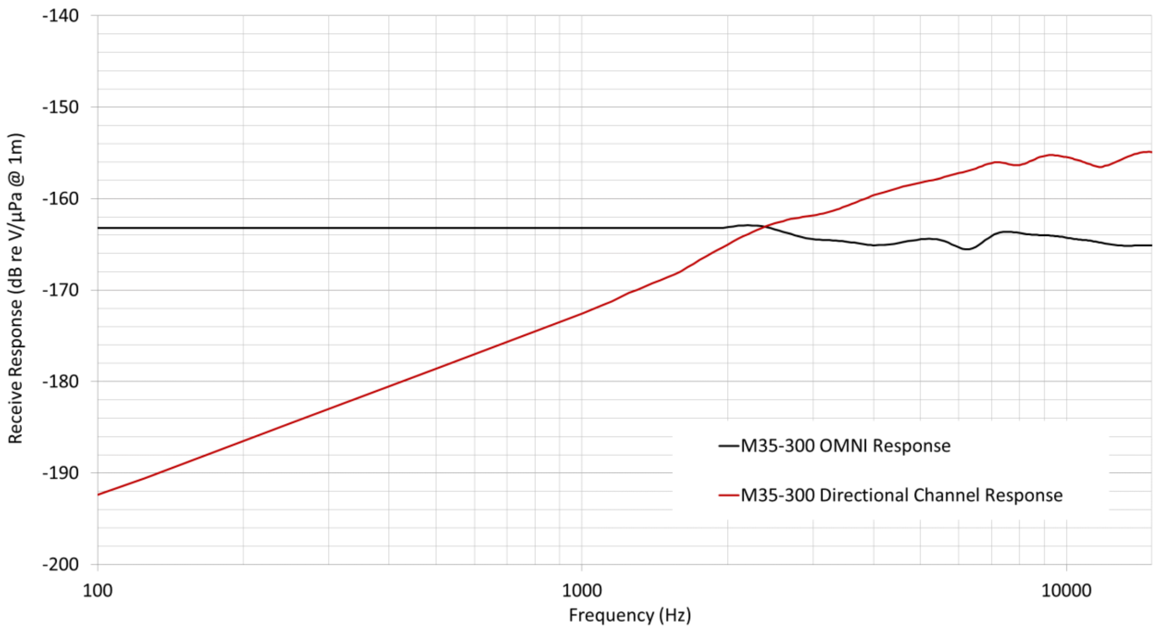

Figure 3: Generic M35-300 receive response with 36 dB gain.

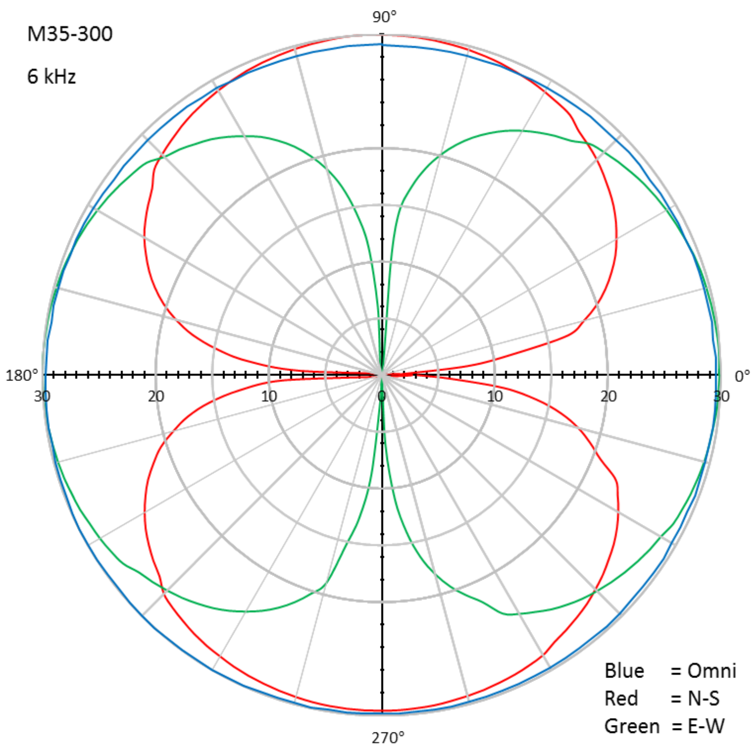

Figure 4: Measured Directivity of M35-300 Directional Hydrophone at 6 kHz.

I.2.3 Autonomous acquisition system

Figure 1.2 shows a simplified structure of the recorder. As shown in the VS manual, the VS preamplifier provides a gain of 36 dB, and the VS outputs are differential signals. The first stage of the recorder is the programmable gain amplifier (PGA), which was set to unitary. The analog-to-digital converter (ADC) is the ADS1278 [11]. This AD is a 24-bit sigma-delta with sampling frequency up to 144 ksps, and its 8-channels are simultaneous-sampling. In the EMSO'21 sea trial, the used sampling frequency is 39062 Hz. The ADC output is normalized to ± 1V (1/5 scaled), which is the range of the recorded signal. The microcontroller is based on the LPC4337 Cortex-M4 (see [12] for a complete description) from where the data are stored into the SD card in .wav format.

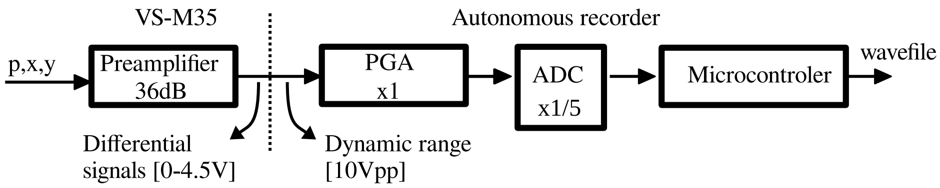

Figure 1.2: Simplified recorder structure

I.2.4 Portable Acoustic Source Unit - PASU

Figure 1.3 shows the Portable Acoustic Source Unit - PASU. This mounted-box power system is used to amplify (according to the impedance matching) the transmission signals that comes from an audio file (for instance, from a laptop). The system is powered by 12V Lithium-ion battery (internal or external). The output cable is connected to the Lubell. During the EMSO'21, the output voltage was about 24V [5 kHz] and 21V [10 kHz].

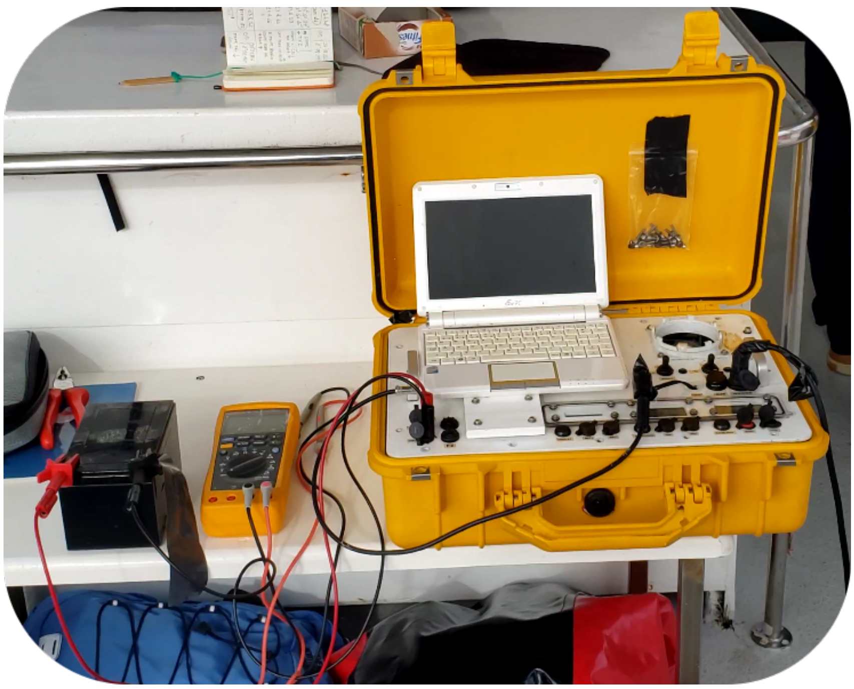

Figure 1.3: Portable Acoustic Source Unit - PASU

I.2.5 CTD

The CTD used in the sea trial is the RBRconcerto. Listing I.1 shows the m-file used to read and plot the CTD data.

Listing I.1: CTD read m-file

```
clear all

data = xlsread('20211124_EMSO_Vilamoura/CTD/ExperienciaFabricio065582_20211124_1434.xlsx','Data','A3:J18882');%file path

data_time = data(:,1);
data_depth = data(:,7);
data_ssp = data(:,10);

indx_ssp_util = find(data_ssp>1510);
indx_break = find(diff(indx_ssp_util)>100);
indx_break(2:length(indx_break)+1) = indx_break;
indx_break(1) = 1;
indx_break(end+1) = length(indx_ssp_util);

figure
way_count = 1;
for uu = 1:length(indx_break)-1
    depth_ax = -data_depth(indx_ssp_util(indx_break(uu):indx_break(uu+1)));
    ssp_ax = data_ssp(indx_ssp_util(indx_break(uu):indx_break(uu+1)));
    subplot(5,3,uu)
    count_dir = 0;
    for kk = 1:length(depth_ax)-1
        if(depth_ax(kk+1)-depth_ax(kk)>0)
            count_dir = count_dir + 1;
        end
        if(count_dir>=100)
            break
        end
    end
    plot(ssp_ax(3:kk-101),depth_ax(3:kk-101))
    time_ssp = datetime(data_time(indx_ssp_util(indx_break(uu+1))),'ConvertFrom','excel');
    [hh,mm,ss] = hms(time_ssp);
    if(hh<10)
        hh_str = strcat('0',num2str(hh));
    else
        hh_str = num2str(hh);
    end
```

```matlab
     if(mm<10)
        mm_str = strcat('0',num2str(mm));
    else
        mm_str = num2str(mm);
     end

    switch uu
        case {1,2,8,9,10},min_ax_vl = 1515.5;
        case {3,4,5,6,7,13,14,15},min_ax_vl = 1516.0;
        case 11,min_ax_vl = 1514.5;
        case 12,min_ax_vl = 1515;
    end

    xlim([min_ax_vl min_ax_vl+1.5]),xticks(min_ax_vl:0.5:(min_ax_vl+1.5))
    text(min_ax_vl+0.3,-3,strcat(hh_str,':',mm_str),'FontSize',14)


    if(uu>2)
        rectangle('Position',[min_ax_vl+0.05 -4.5 0.25 4],'Curvature',[1,1],'FaceColor',[1 1 1])
        text(min_ax_vl+0.1,-3,strcat('',num2str(way_count)),'FontSize',14)
    end
    ylim([-20 0])

    if(uu==1 || uu==4 || uu==7 || uu==10 || uu==13)
        ylabel('depth~(m)')
    end
    if(uu>=13)
        xlabel('speed~(m/s)')
    end
    if(uu > 2)
    way_count = way_count + 1;
    end
    if(way_count == 5)
        way_count = way_count + 1;
    end
    grid on

    line([1516 1516],[-20 0],'Color','red')
end
```

A sample of the CTD express manual is shown in the following pages. One can find the full technical characteristic in [13].

Container description

The container is composed by:

- 1 CTD Ruskin Concerto
- 1 O_2 sensor ARO-CAV
- 3 Supports
- 1 O_2 sensor to CTD connector
- 1 CTD Ruskin Concerto to USB connector

Figura 1: Complete container.

CTD Ruskin Concerto

The CTD Ruskin Concerto is a watertight cylindrical tube used in underwater measurements to evaluate the water conductivity, temperature and depth (Figura 2). Along with these sensors, the equipment is composed by an internal module that include electronics, battery and data storage. Additionally Ruskin Concerto permits to connect an O_2 sensor.

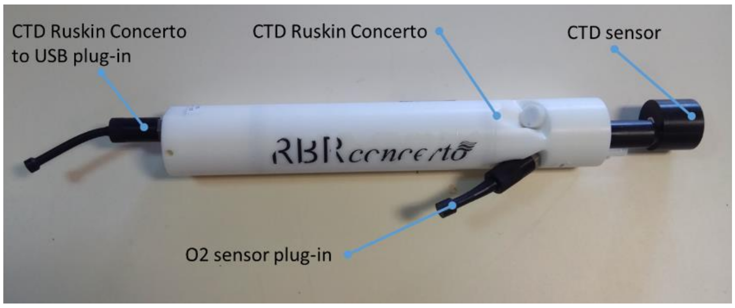

Figura 2: CTD Ruskin Concerto part description.

To open the container one needs to hold the container with the sensor pointing up and lightly unscrew it by hand, turning the lower part clockwise and the upper part of the container counter-clockwise. Slowly slide off the container and place the internal electronics horizontally in a secure position.

To connect the CTD Ruskin Concerto to your computer unscrew and pull the protection cover on the rear side and connect CTD Ruskin Concerto to USB plug-in (Figura 3).

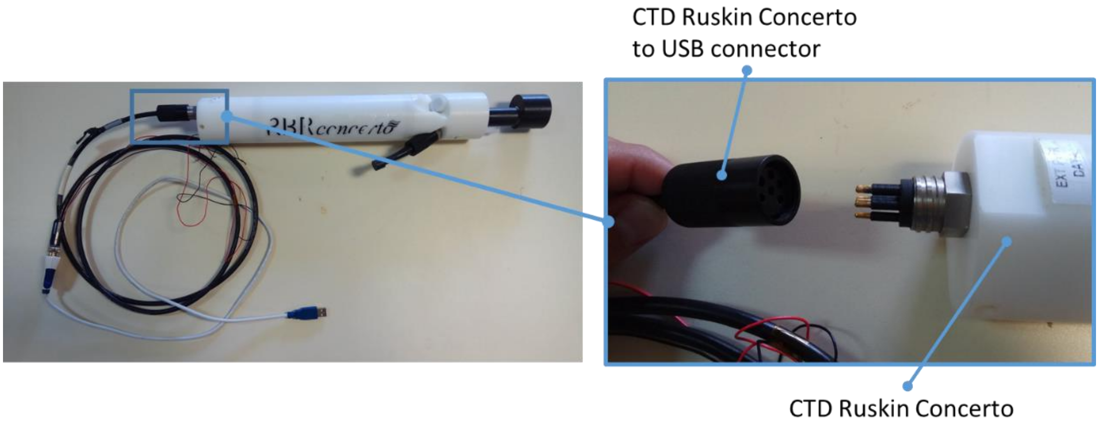

Figura 3: Connecting Ruskin Concerto to PC.

Once the USB connector is plugged, it is possible to program the CTD and start measuring. The programming description step will be described in the following sections.

Connecting the O_2 sensor

To connect the O_2 sensor it is necessary to unscrew and pull the protection cover on the CTD Ruskin Concerto frame and connect the O2 to CTD connector/cable and then plug the sensor (Figura 4).

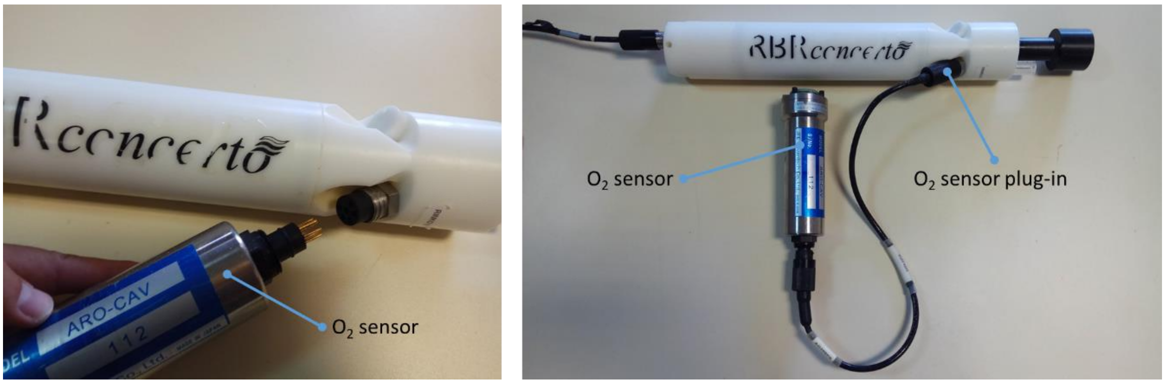

Figura 4: Connecting the O_2 sensor.

Note: **DO NOT** force to connect the O_2 sensor to the CTD. The O2 plug has a guiding pin to correctly place it that should be respected (Figura 5).

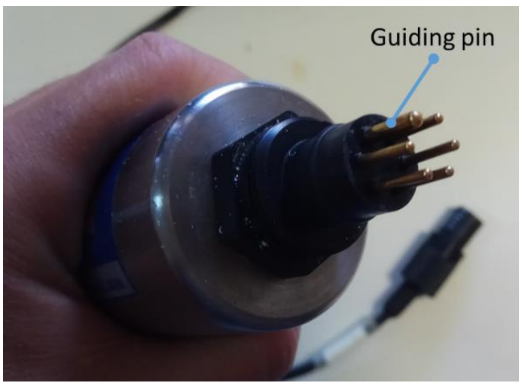

Figura 5: O_2 guiding pin.

I.3 Project folder structure

Figure 1.4 shows the folder structure with the main files highlighted.

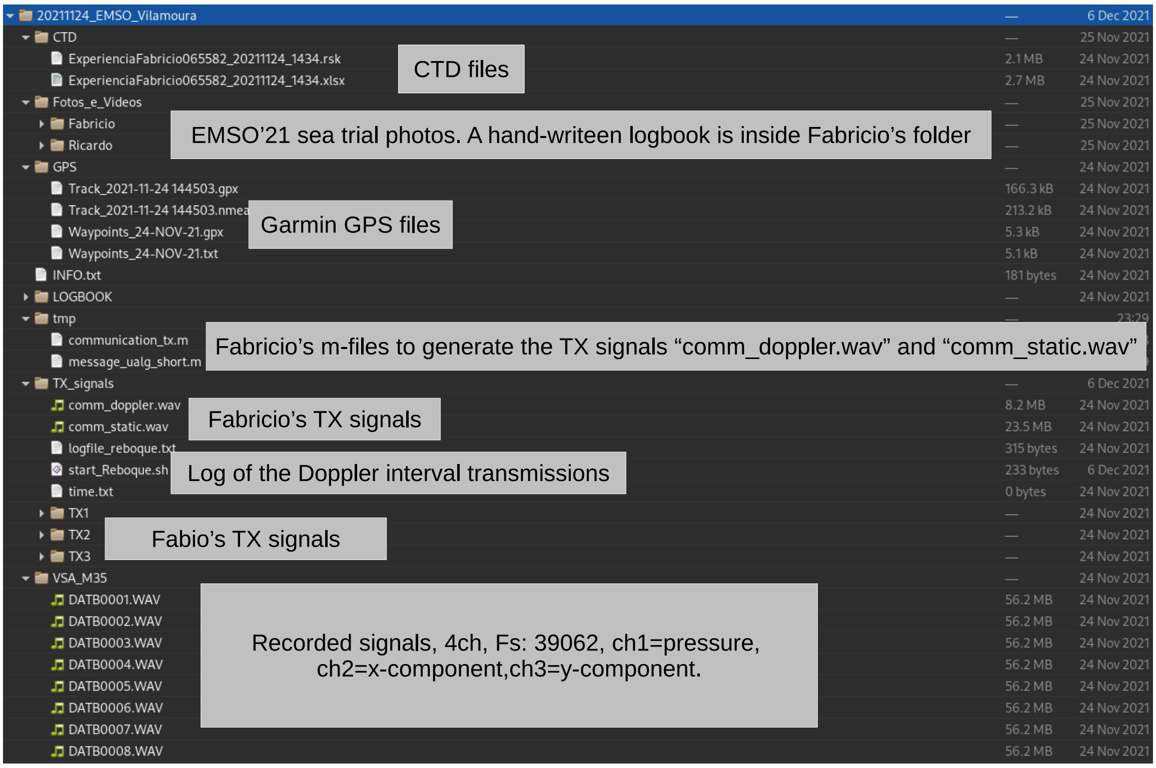

Figure 1.4: Folder structure

Annex II

Channel Impulse Response

II.1 CIR - Communication test 1

The CIR was calculated using the first 500 symbols preamble. CIR snapshot (delay) was obtained for each 1 s. Thus, we have 50 s (time or geotime) time-varying CIR. From top to bottom represent different BPSK configuration being respectively: [3 kHz-7 kHz] 255 m-seq, [8 kHz-12 kHz] 255 m-seq, [3 kHz-7 kHz] 127 m-seq, [8 kHz-12 kHz] 127 m-seq.

The estimated channel impulse response for each station and each BPSK configuration are present in Figs. 2.1 to 2.14. Those CIR (40 ms) were estimated using a bank of correlators and using a 250 ms preamble. In summary, we notice severe fading, even in the morning interval, where the sea was really flat. We have opted to normalize the channels to the maximum for a better visualization, and except for station 6, the channels seem to be very similar (future correlation analysis is necessary to confirm this).

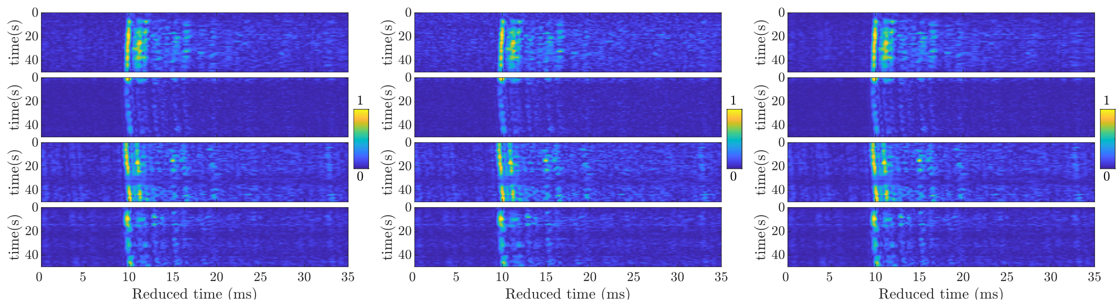

(a) CIR pressure (b) CIR x-component (c) CIR y-component

Figure 2.1: Channel Estimation station 1

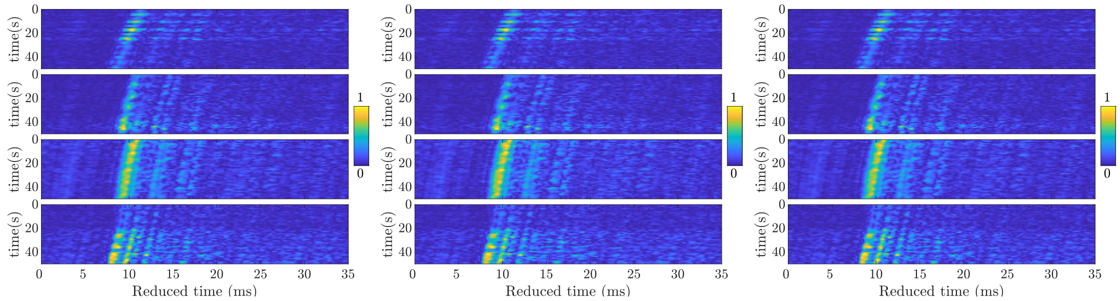

(a) CIR pressure (b) CIR x-component (c) CIR y-component

Figure 2.2: Channel Estimation station 2

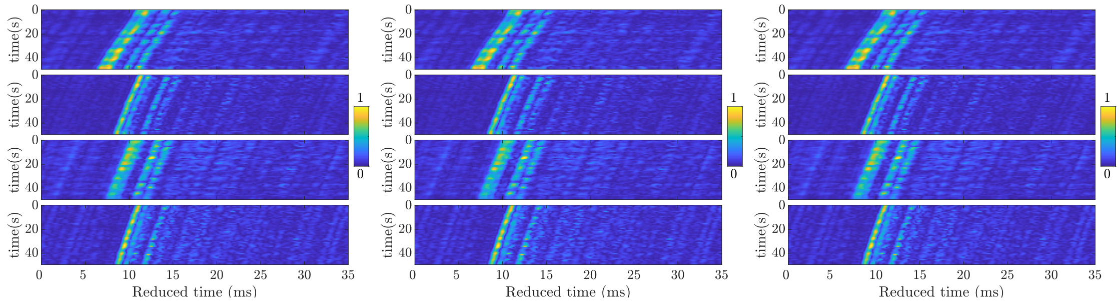

(a) CIR pressure (b) CIR x-component (c) CIR y-component

Figure 2.3: Channel Estimation station 3

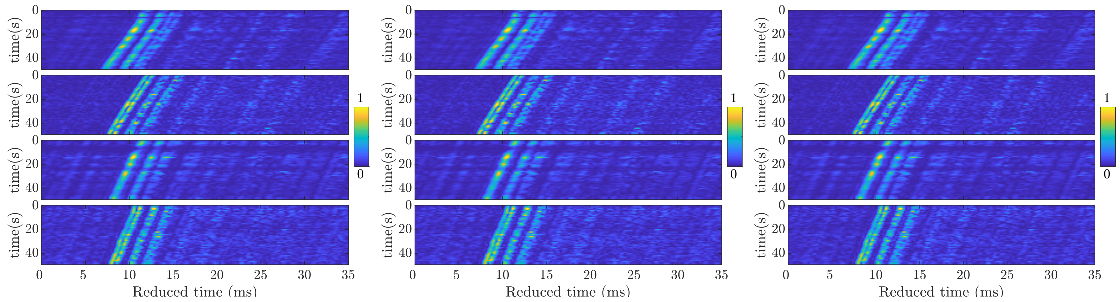

(a) CIR pressure (b) CIR x-component (c) CIR y-component

Figure 2.4: Channel Estimation station 4

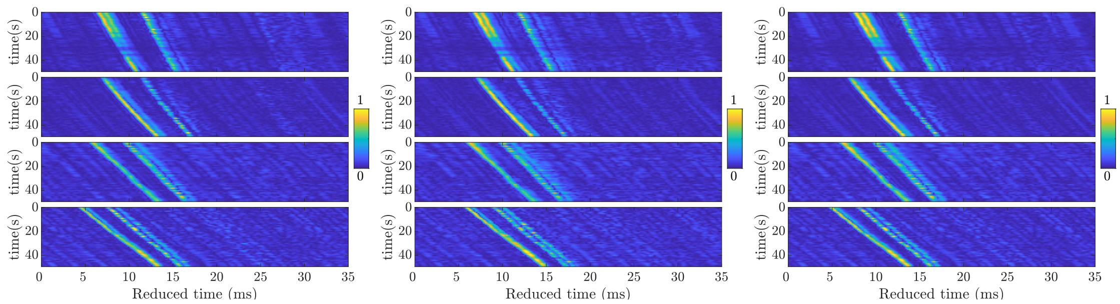

(a) CIR pressure (b) CIR x-component (c) CIR y-component

Figure 2.5: Channel Estimation station 5

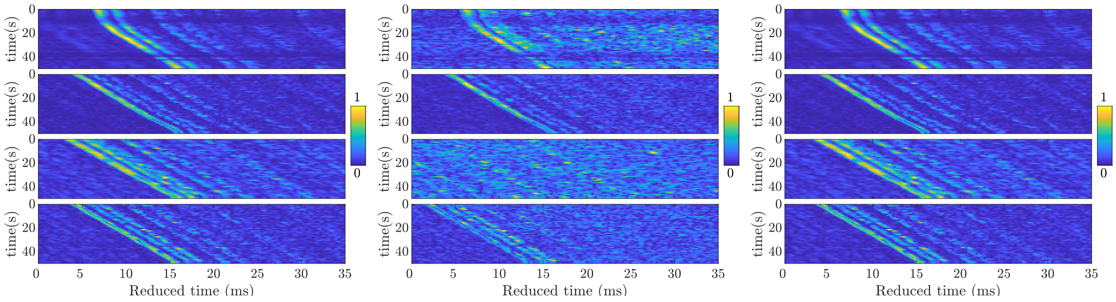

(a) CIR pressure (b) CIR x-component (c) CIR y-component

Figure 2.6: Channel Estimation station 6

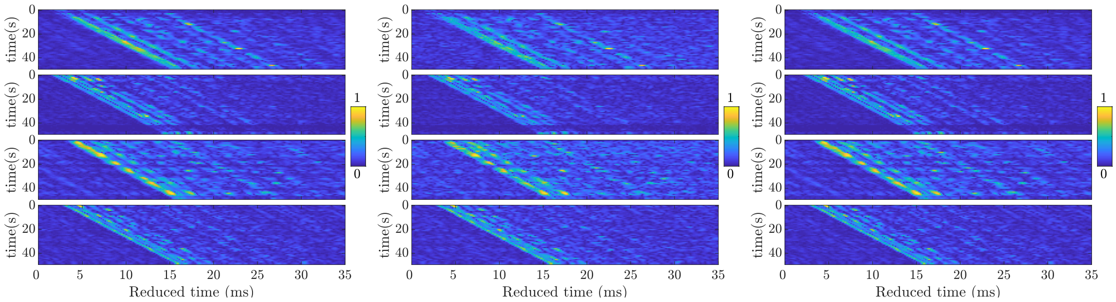

(a) CIR pressure (b) CIR x-component (c) CIR y-component

Figure 2.7: Channel Estimation station 7

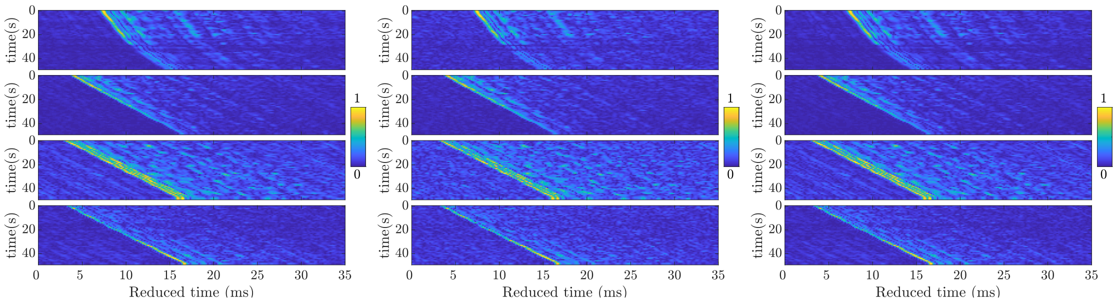

(a) CIR pressure (b) CIR x-component (c) CIR y-component

Figure 2.8: Channel Estimation station 8

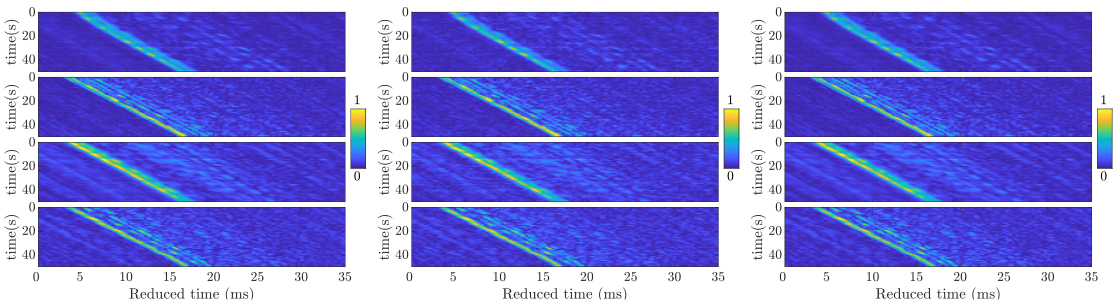

(a) CIR pressure (b) CIR x-component (c) CIR y-component

Figure 2.9: Channel Estimation station 9

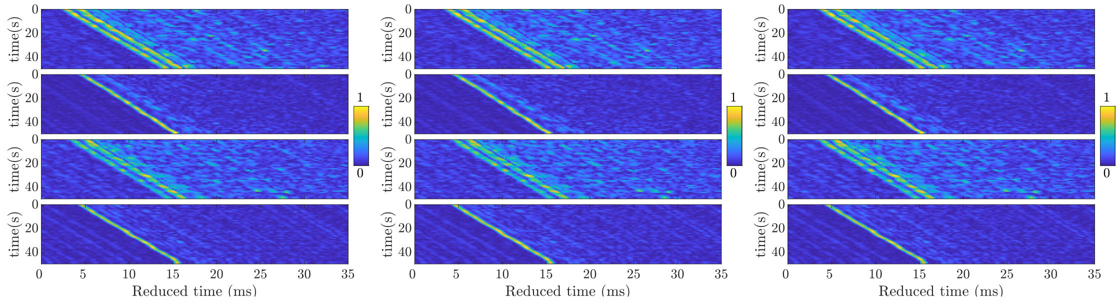

(a) CIR pressure (b) CIR x-component (c) CIR y-component

Figure 2.10: Channel Estimation station 10

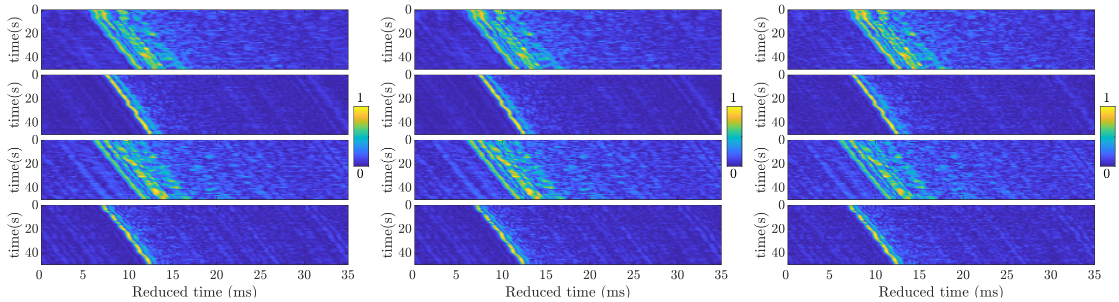

(a) CIR pressure (b) CIR x-component (c) CIR y-component

Figure 2.11: Channel Estimation station 11

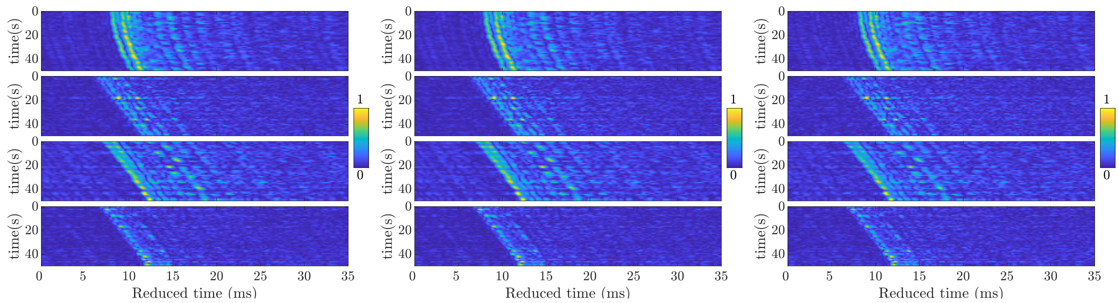

(a) CIR pressure (b) CIR x-component (c) CIR y-component

Figure 2.12: Channel Estimation station 12

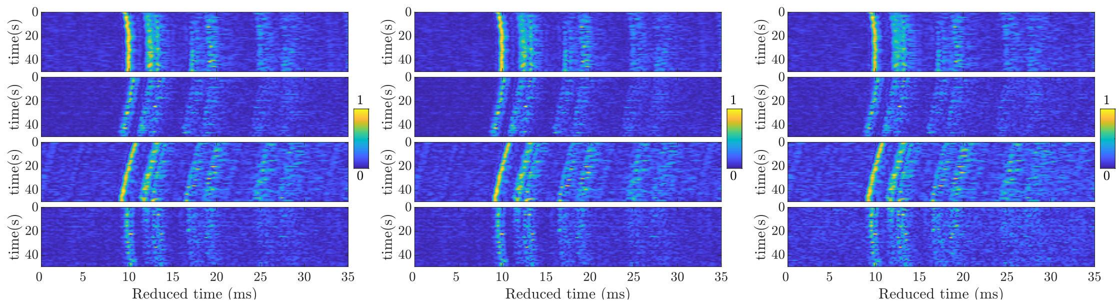

(a) CIR pressure (b) CIR x-component (c) CIR y-component

Figure 2.13: Channel Estimation station 13

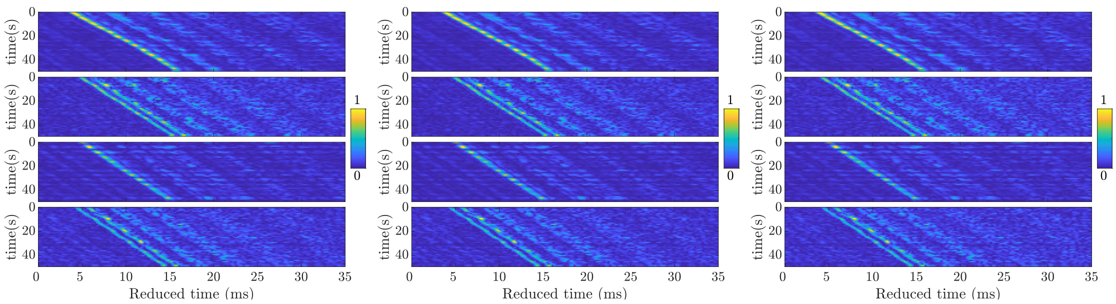

(a) CIR pressure (b) CIR x-component (c) CIR y-component

Figure 2.14: Channel Estimation station 14

II.2 CIR - Communication test 2

The CIR was calculated using the first 255/127 symbols preamble. CIR snapshot (delay) was obtained for each 1 s. Thus, we have 10 s (time or geotime) time-varying CIR. From top to bottom represent different BPSK configuration being respectively: [3 kHz-7 kHz] 255 m-seq, [8 kHz-12 kHz] 255 m-seq, [3 kHz-7 kHz] 127 m-seq, [8 kHz-12 kHz] 127 m-seq.

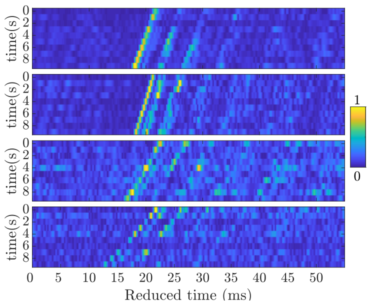

(a) CIR pressure

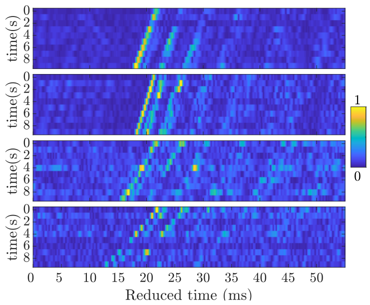

(b) CIR x-component

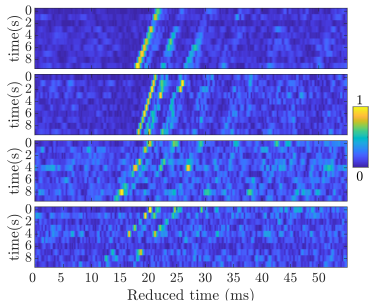

(c) CIR y-component

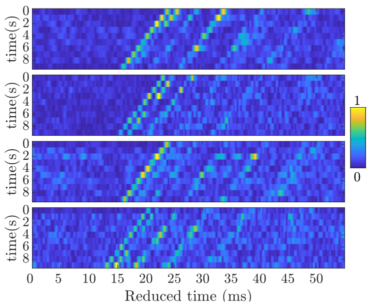

(d) CIR pressure

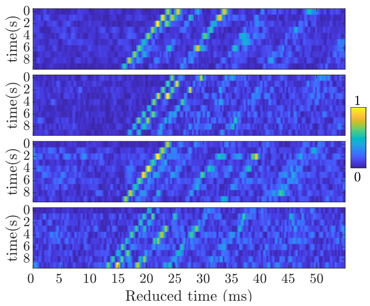

(e) CIR x-component

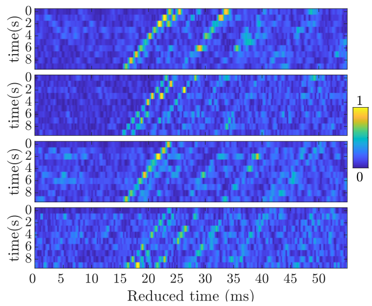

(f) CIR y-component

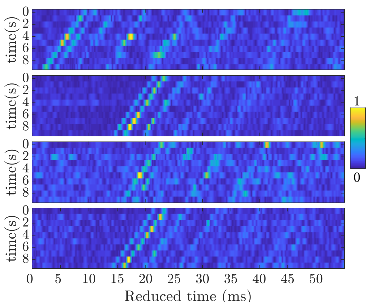

(g) CIR pressure

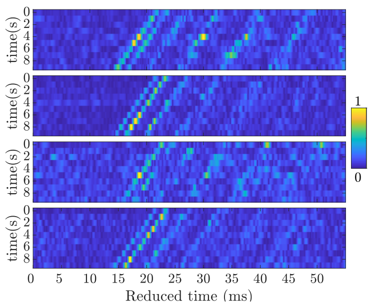

(h) CIR x-component

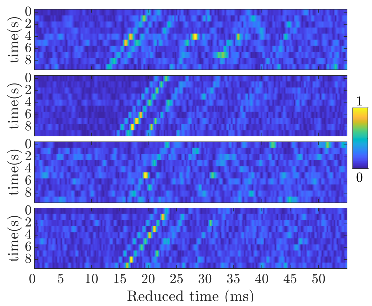

(i) CIR y-component

Figure 2.15: Channel Estimation Doppler

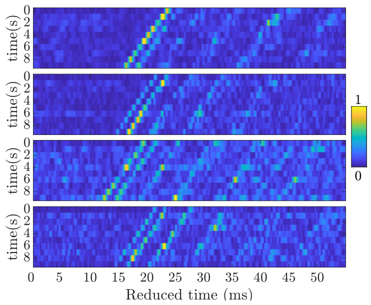

(j) CIR pressure

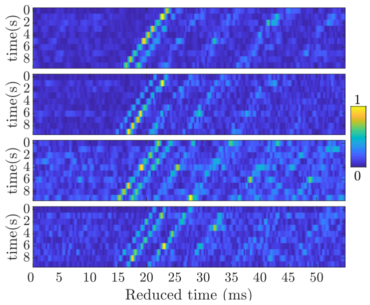

(k) CIR x-component

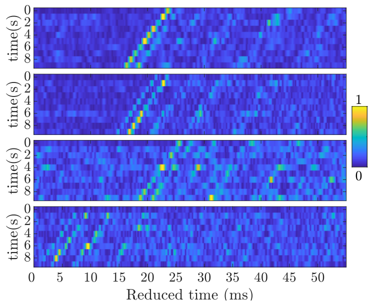

(l) CIR y-component

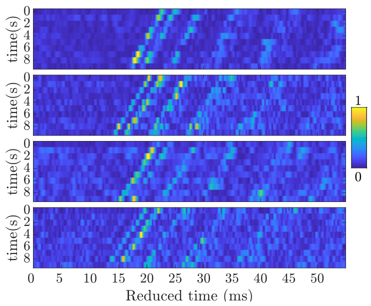

(m) CIR pressure

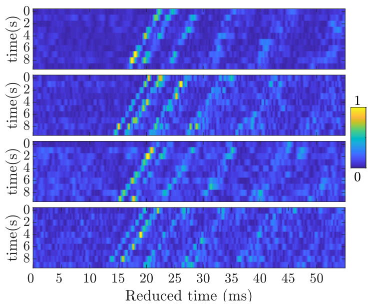

(n) CIR x-component

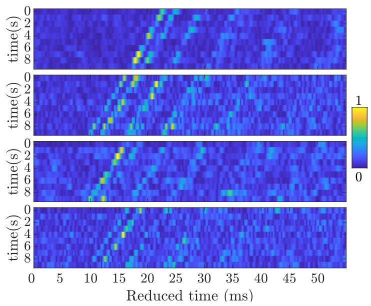

(o) CIR y-component

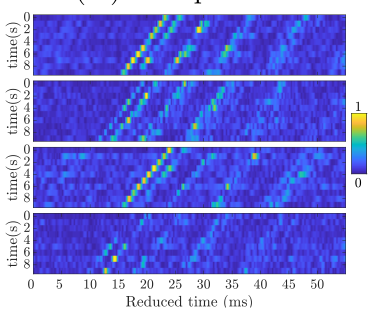

(p) CIR pressure

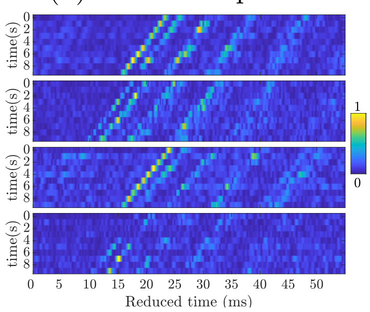

(q) CIR x-component

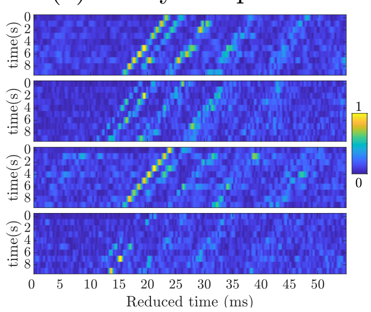

(r) CIR y-component

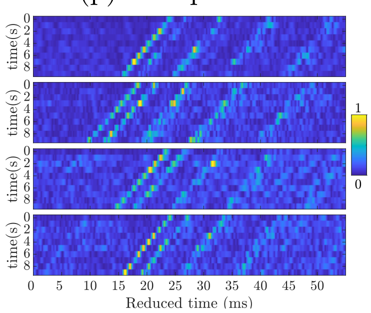

(s) CIR pressure

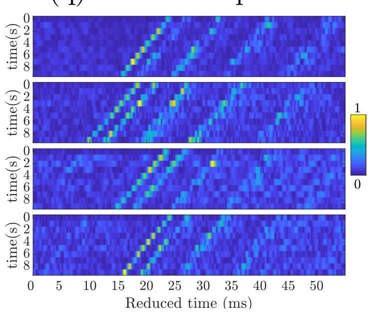

(t) CIR x-component

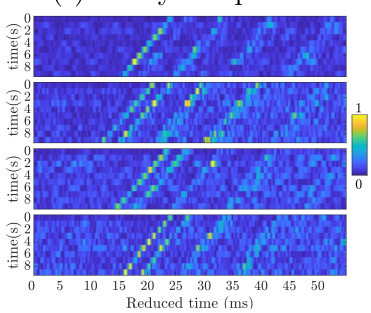

(u) CIR y-component

Figure 2.15: Channel Estimation Doppler

Bibliography

[1] Sandra Sendra, Jaime Lloret, Jose Miguel Jimenez, and Lorena Parra. Underwater Acoustic Modems. *IEEE Sensors Journal*, 16(11):4063–4071, June 2016.

[2] Bas Binnerts, Ingrid Mulders, Koen Blom, Mathieu Colin, and Henry Dol. Development and Demonstration of a Live Data Streaming Capability Using an Underwater Acoustic Communication Link. In *2018 OCEANS - MTS/IEEE Kobe Techno-Oceans (OTO)*, pages 1–7, Kobe, May 2018. IEEE.

[3] Mandar Chitre, Shiraz Shahabudeen, and Milica Stojanovic. Underwater Acoustic Communications and Networking: Recent Advances and Future Challenges. *Marine Technology Society Journal*, 42(1):103–116, March 2008.

[4] T. C. Yang. A study of spatial processing gain in underwater acoustic communications. *IEEE Journal of Oceanic Engineering*, 32(3):689–709, July 2007.

[5] A. Nehorai and E. Paldi. Acoustic vector-sensor array processing. *IEEE Transactions on Signal Processing*, 42(9):2481–2491, September 1994.

[6] J.C. Nickles, G. Edmonds, R. Harriss, F. Fisher, W.S. Hodgkiss, J. Giles, and G. D'Spain. A Vertical Array Of Directional Acoustic Sensors. In *OCEANS 92 Mastering the Oceans Through Technology*, volume 1, pages 340–345, Newport, RI, 1992. IEEE.

[7] Thomas Gabrielson. Design problems and limitations in vector sensors. Proceedings of the Workshop on Directional Acoustic Sensors, Naval Undersea Warfare Center Division and Office of Naval Research, Newport, Rhode Island, April 2001.

[8] Bruce Armstrong. M35-300 Directional Hydrophone. Manual 2018-468, GeoSpectrum Technologies Inc., 10 Akerley Boulevard, Unit 19, Dartmouth, Nova Scotia B3B 1J4, April 2020.

[9] Charles H. Sherman and John L. Butler. *Transducers and arrays for underwater sound*. Monograph series in underwater acoustics. Springer, New York, 2007.

[10] Bruce Armstrong. Directional Hydrophones. Technical Document 2018-464, GeoSpectrum, 10 Akerley Blvd, Unit 19,Dartmouth, Nova Scotia, Canada, B3B 1J4, May 2018.

[11] ADS1278 - 24-Bit, 144kSPS, 8-Ch Simultaneous-Sampling Delta-Sigma ADC for Wide Bandwidth Applications, Online: https://www.ti.com/product/ADS1278, accessed 02-February-2022.

[12] N. Pinto and S.M. Jesus. Calibration of Dual Accelerometer Vector Sensor (DAVS2) at the Alfeite Arsenal Tank. Technical Report 05/20, CINTAL - University of Algave, Campus de Gambelas, 8005-139, Faro, Portugal, July 2020.

[13] Ruskin User Guide Datalogger Manual; Online: http://www.cen.ulaval.ca/RBR_ruskin_datalogger, accessed 02-February-2022, February 2011.